A critical review of the Stark widths and shifts of spectral lines from non-hydrogenic atoms

N. Konjevic, and J. R. Roberts

View Online   Export Citation

ARTICLES YOU MAY BE INTERESTED IN

A Critical Review of the Stark Widths and Shifts of Spectral Lines from Non-Hydrogenic Atoms

N. Konjevic*

Institute of Physics, 11001 Beograd, P. O. Box 57, Yugoslavia

and

J. R. Roberts

Institute for Basic Standards, National Bureau of Standards, Washington, D.C. 20234

A critical review of all available data on the Stark broadening and shifts of spectral lines of neutral elements has been undertaken. Over 200 papers compiled by the NBS Data Center on Atomic Line Shapes and Shifts have been evaluated, and of these, 68 were chosen as having reviewable data. Only those papers with properly determined critical factors, such as electron density, temperature, spatial homogeneity, optical depth, and instrument function deconvolution, were selected.

Key words: Experimental; neutral atom; review; shift; Stark broadening; width.

Contents

1. Introduction

It should be emphasized at the outset that this is primarily a review of experimental results, i.e., theory is used only as a check for experimental consistency within experiments and between different experiments. For this reason the theory with the most comprehensive calculations was chosen [1].[1]

The basis for the experimental review was a comprehensive bibliography on atomic line shapes and shifts [2]. This is an exhaustive list of all atomic spectral line broadening literature from 1889 through 1973 and con-

[1] Figures in brackets indicate the literature references in section 6, not to be confused with individual element references.

tains over 1750 references. A few additional references are included from the up-to-date compilations of the Data Center on Atomic Line Shapes and Shifts at NBS.

To summarize what was included in this review on the Stark broadening of neutral atomic lines, the following statistics are given. Over 200 references were reviewed, and of these, 68 were chosen. There were 19 elements with at least one experimental result. Seven elements, however, had only one reviewable experiment. The elements Be, B, Al, and K had theoretical results [1], but there were no reviewable experimental results for comparison, whereas Ge, Xe, Cd, and Zn had experimental results but no theoretical comparison.

The two Stark broadening parameters that were taken from each experiment were the total halfwidth, i.e., the total width of the spectral line at one-half its peak intensity and the shift of the spectral line's peak intensity wavelength. The shift is given by $\lambda-\lambda_0$; therefore, a positive shift is when the measured peak intensity wavelength has shifted to longer wavelengths (red) and a negative shift is to shorter wavelengths (blue).

It is the intention of the staff at the NBS Data Center on Atomic Line Shapes and Shifts to undertake or commission future critical reviews on this subject when major changes, additions, and improvements in the body of data warrant it.

2. Review Criteria

To arrive at the results of the review, certain criteria were imposed on each experimental paper. Not all experiments reviewed are included in the final results. The criteria imposed were as follows:

(a) An independent and accurate determination of the plasma electron density, N_e.

(b) A reasonably accurate determination of the plasma temperature.

(c) A discussion of other interfering broadening mechanisms and appropriate experimental problems.

The importance of an accurate and independent electron density measurement cannot be overemphasized because the Stark shift and width of isolated spectral lines are directly proportional to N_e. They are not nearly as sensitive a function of the temperature, however. Therefore, this measurement is not as critical, but the temperature should still be determined within a ±10 percent uncertainty to give a reasonable accuracy to the Stark width and shift measurements. As will be discussed later for lines which have comparable Stark and Doppler widths, the determination of the plasma temperature is important for the deconvolution of these two competing broadening mechanisms. Included in these criteria should perhaps be another one—the proper presentation of the experimental data. Many papers were excluded from this review because the data were in a form that was impossible to reduce to simple widths and/or shifts.

Experimental problems and other broadening mechanisms are often times very critical to the proper determination of Stark parameters, but some are over-

looked or improperly accounted for. To break down these review criteria in more detail, we will first look at the critical plasma parameters of electron density and temperature and review some of the ways they are determined. For reasons of brevity, this will be done only in a cursory manner, since most of these subjects are covered in detail in a number of books on plasma spectroscopy, e.g., [3–5].

2.1. Electron Density

a. Stark Widths

Often times Stark widths of other atoms (or ions) are used to determine the plasma electron density. Prime among these is hydrogen, especially the hydrogen Balmer lines. This has been demonstrated by detailed experiments [1, 3, 6].

Helium and ionized helium are also good candidates for higher temperature plasmas, but experimental results compared with theory indicate the lines of neutral helium may be less reliable as an electron density probe and thus give a larger uncertainty in N_e than hydrogen, e.g., see review table on helium.

b. Absolute Line or Continuum Intensities

This method for the determination of electron densities depends critically on an absolute spectral radiance calibration. In the case of spectral lines it also depends on the knowledge of the absolute transition probability of the line as can be seen from eq (1) for the case of optically thin line emission. The total line intensity I is given by

$$I = h\nu_{ul}A_{ul}N_ul,   \tag{1}$$

where N_u is the density of atoms in the upper state, A_{ul} is the absolute transition probability for spontaneous emission, l is the emitting length, and ν_{ul} is the emission frequency of the line. Through equilibrium relations, N_e may be related to N_u and thus I for both the line and continuum radiation. One of the most critical problems in obtaining reliable electron densities from absolute line intensities is the assumption and validity of an equilibrium relation, e.g., the Saha-Boltzmann relations to connect upper state densities with the density of free electrons. Validity criteria and experimental studies have specified the range of densities and temperatures where thermal equilibrium is valid. Another important point is the ability of the experimental apparatus to measure the total integrated line intensity in the presence of a background continuum and/or other spectral lines. This is demonstrated in ref. [5], chap. 6, p. 311.

To determine the electron density from continuum intensities, the free-free and free-bound contributions from all species must be known, e.g., H, H⁻, H_2^+ in the case of the hydrogen continuum [7], as well as the corresponding "Gaunt" factors or ξ factors for a non-hydrogenic continua (e.g., see ref. [4]). An equilibrium relation is also necessary for the determination of electron density from continuum intensities.

c. Inglis-Teller Limit

This method of electron density determination relates the last observable line of a spectral series to the electron density, i.e.,

$$\log N_e = 23.26 - 7.5 \log n_{max}, \tag{2}$$

where N_e is the electron density and n_{max} is the upper principal quantum number of the last observed line. This method is not too useful at high electron densities, e.g., in an atmospheric hydrogen arc plasma at $N_e \sim 10^{17}$ cm^{-3} [6], n_{max} changes from 7 to 6 which changes N_e by more than a factor of 3.

d. Interferometry

The use of interferometry to determine electron density is based on the principle that the plasma's refractive index is predominantly determined by free electrons. The change in the index of refraction is related to the shift of an interference fringe, but the refractive index is also related to the electron, atomic, and molecular densities (e.g., see ref. [4]). This method has some disadvantages, namely, knowledge of the effective plasma length and plasma nonhomogeneities, among others, but has the advantage like the Stark width method of not depending on equilibrium relations and/or temperature.

2.2. Temperature

a. Doppler Widths

For a Doppler broadened spectral line, the intensity distribution is Gaussian and is given by

$$I(\Delta\lambda) = \frac{I_o}{\sqrt{\pi}\Delta\lambda_D} \exp\left[-(\Delta\lambda/\Delta\lambda_D)^2\right], \tag{3}$$

where I_o is the integrated line intensity and $\Delta\lambda_D$ is the Doppler width which is related to the full width at one-half the maximum line intensity, $\Delta\lambda_{1/2}$, by

$$\Delta\lambda_{1/2} = 2 (\ln 2)^{1/2} \Delta\lambda_D$$
$$= 7.162 \times 10^{-7} \lambda(T/\mu)^{1/2}, \tag{4}$$

where λ is the line wavelength in Å, T is the temperature in K, and μ is the atomic weight. This method of temperature determination is not too useful in high density-low temperature plasmas because the Stark width of a line usually predominates (see section on competing effects) or other broadening mechanisms interfere. Turbulent plasma effects may also cause interfering broadening. It does have one unique feature in that it determines the kinetic temperature of the atoms or ions instead of the electron temperature.

b. Absolute and Relative Line Intensities

Since the line intensity for an optically thin plasma is proportional to the number density of the upper state, through equilibrium relations, one can obtain a temperature from the measurement of this intensity. In the case of absolute line intensities, one must also have knowl-

edge of the absolute transition probability and the plasma emitting length, and an absolute spectral radiance calibration must be performed. This can be seen from eq. (5) for the case of Boltzmann equilibrium.

$$I = h\nu_{ul}g_u A_{ul}\, l\, \frac{N_o}{Z}\, e^{-E_u/kT}, \tag{5}$$

where ν_{ul}, A_{ul}, and l are the same as explained in eq. (1), N_o is the total number density in cm^{-3} of the radiating species, E_u is the upper state energy, T is the temperature, g_u is the upper state degeneracy and equals $2J_u + 1$ (J_u is the upper state total angular momentum), and Z is the partition function. For relative line intensities of the same species and stage of ionization, besides the equilibration assumption (usually partial LTE), only relative transition probabilities and a relative spectral radiance calibration are needed to determine temperature. But because this method of relative line intensities depends on the difference in upper state energies, it is quite insensitive for lines within the same stage of ionization when this energy difference is small compared with kT, as demonstrated in eq. (6),

$$\frac{I_1}{I_2} = \frac{(gA)_1\,\lambda_2}{(gA)_2\,\lambda_1} \exp[(E_2 - E_1)/kT], \tag{6}$$

where 1 and 2 denote two different transitions within the same species and stage of ionization.

For lines of different stages of ionization of the same species, this method can be very sensitive because the energy difference is usually quite large, but because of the equilibrium assumption, usually Saha equilibrium, this method also depends on an independent knowledge of the electron density and depends strongly on LTE, as shown in eq (7) for Saha-Boltzmann equilibrium.

$$\frac{I_1}{I_2} = \frac{h^3}{2(2\pi mk)^{3/2}} \frac{(gA)_1\,\lambda_2\,N_e}{(gA)_2\,\lambda_1\,T^{3/2}}$$
$$\times \exp(E_2 - E_1 + E_1{}^{ion} - \Delta E)/kT, \tag{7}$$

where 1 and 2 denote two transitions within the same species but consecutive stages of ionization, N_e is the electron density (cm^{-3}), T is the temperature (K), E_2 and E_1 are the excitation energies, $E_1{}^{ion}$ is the ionization potential of the lower stage of ionization, and ΔE is the lowering of the ionization potential (e.g., see ref. [3]).

c. Absolute and Relative Continuum Intensities

An example of the application of relative continuum intensity to determine temperature is the use of the intensity ratio across the so-called "Balmer discontinuity" in hydrogen plasmas [3], chap. 13, and [8]. Use of this method depends on a knowledge of the theoretical relative intensity distribution of the continuum under investigation [7] and is used mainly in pure gases. In the absolute intensity case, the temperature determination is dependent on an absolute spectral radiance calibration, the theoretical absolute intensity distribution (see, e.g., ref. [7]), and an independent electron density determination.

d. Relative Line-to-Continuum Intensities

For this case, as in the relative continuum intensity, this method to determine temperature is normally used for pure gases. Knowledge of the line transition probability and the continuum Gaunt factors are necessary, and this method is not dependent on an electron density determination but is dependent on an equilibrium assumption. There are many examples of this method throughout the literature where the ratio of a Balmer line intensity to 100 Å of hydrogen continuum is measured (e.g., ref. [3]). In the case of hydrogen, all theoretical dependencies are well known and have been calculated so this ratio is quite accurately known.

e. Fowler-Milne Method

This method of temperature determination defines the temperature at the point where the slope of the line intensity-versus-temperature curve is zero (for a constant pressure). It involves only a relative line intensity and depends on equilibrium relations to give the temperature and also the density of electrons. It has the disadvantage that near this maximum the slope of the intensity-versus-temperature curve changes quite slowly; therefore, the temperature has a relatively large uncertainty if only the zero slope point is measured. However, if the intensity-versus-temperature curve is measured on both the high and low temperature sides of its maximum and a fit is made, this method can be quite accurate.

f. Optically Thick Lines

Up to this point, an optically thin plasma has been assumed for all diagnostic methods. In this example of temperature determination, there is a line (or lines) whose peak intensity is equal to the blackbody intensity at the plasma temperature. This peak intensity is independent of transition probabilities and is simply described by Planck's law. An absolute intensity calibration and the assumption of LTE are also necessary, however. The major problem with this method is that this blackbody radiation may arise from layers at different temperatures, e.g., nonhomogeneous plasmas or plasmas with boundary layers, and the resultant intensity does not correspond to the homogeneous, optically thick plasma that was assumed under investigation.

An additional method that relies on the absorption of radiation to determine temperature is the line reversal method. This technique utilizes a variable-intensity (calibrated), usually continuous, light source that backlights the emission from the plasma. When the temperature of the calibrated continuous source equals the temperature of the plasma, i.e., the total intensity of the plasma plus the back lighting source equals the intensity of the blackbody at the plasma temperature, the plasma spectral line goes from an emission line to an absorption line. Since the reversal method depends only on the population ratio of the levels within an atomic species, if spectral lines arising from different excitation poten-

tials all give the same reversal temperature, this allows one to attribute Boltzmann equilibrium to these excited levels of this species.

Many other methods of determining electron density and temperature exist and are discussed in detail in refs. [3] and [4], e.g., the curve-of-growth method to determine plasma densities, the determination of temperature from the sound velocity, and the determination of densities from plasma refractivity using the Schlieren method.

2.3. Experimental Problems and Competing Effects

For the sake of brevity and because some of these points are covered in detail elsewhere [1, 3–5], all pertinent problems will be listed, but only a few will be discussed in any detail.

a. Plasma Stability and Homogeneity

As one example of stability and homogeneity, the problems associated with transient sources will be discussed. Because of their basic transient nature, care must be taken to assure that these sources do not have any inhomogeneities due to instabilities or boundary layers. Also, because line profiles are sometimes scanned using data obtained by repetitively discharging the source while incrementally stepping the wavelength of a monochromator, care must be taken that all data are taken at the same electron density and as closely as possible at the same temperature. This requires a very reproducible transient source. By careful design and reproducible experimental conditions, such as filling pressure and charging voltage, transient electrical discharge sources such as the "T-tube" and the pulsed arc, among others, have fulfilled these homogeneity and stability requirements to within a ±15 percent uncertainty and have provided reliable Stark broadening data. Conventional gas-driven shock tubes have also provided reliable results, but again inhomogeneities such as boundary layers and turbulences (especially in the multiply reflected shock region) must be kept to a minimum if reliable data are to be obtained.

The radial intensity distribution of stationary sources such as arcs (both wall-stabilized and free-burning) and plasma jets, among others, make it necessary to mathematically unfold this distribution in order to get the most accurate Stark broadening data from such sources. Fortunately, because they are stationary, these sources lend themselves to radial scans of this intensity distribution in order that plasma parameters, such as electron density and temperature, can be unfolded. This is done by the Abel inversion process which has been widely discussed (see, e.g., ref. [4]). The general distributional features of stationary and transient sources are shown in figure 1. In table 1 is a list of various types of sources and typical operating ranges of electron density and temperature.
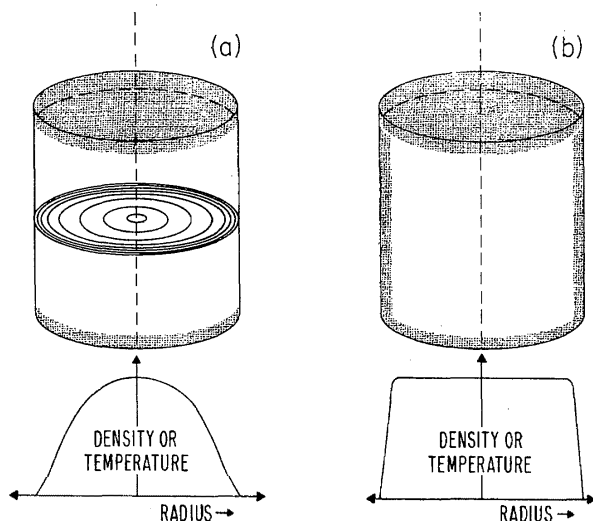
FIGURE 1. Distributional features of stationary (a) and transient (b) sources.

TABLE 1. Sources and operating ranges of N_e and T

Type	N_e (cm^{-3})	Temp. (K)
(Homogeneous)		
1. Shock tubes	$10^{14} - 10^{18}$	$5000 - 20000$
2. Pulsed discharges	$10^{14} - 10^{18}$	$5000 - 1000000$
3. Ovens (end-on)	$< 10^{15}$	< 3000
4. Wall-stabilized arc (end-on)	$10^{16} - 2 \times 10^{17}$	$10000 - 25000$
(Nonhomogeneous)		
1. Wall-stabilized arc (side-on)	$10^{15} - 10^{17}$	$10000 - 20000$
2. Free-burning arc	$10^{15} - 10^{17}$	$5000 - 20000$
3. Vortex stabilized arc	$10^{16} - 10^{17}$	$10000 - 20000$
4. R-F discharges	$10^{13} - 10^{16}$	$1000 - 10000$
5. Plasma jet	$10^{16} - 10^{17}$	$10000 - 20000$

b. Recording Method

The two major methods used in obtaining experimental data on the widths and shifts of spectral lines are the photoelectric and photographic techniques. Because of the greater range of linear response and ease of data processing and handling, the photoelectric technique is most suitable for line profile measurements, especially on stationary sources. The response of photoelectric detectors is linear over approximately a factor of 10^5 (even for transient sources [8]). In the photographic technique, the characteristic curve (film density versus log exposure) is linear over approximately a factor of 10^2 to 10^3, and because of the possibility for time integrating the signal, thus improving the signal-to-noise ratio, this technique is especially useful in shift measurements. The more limited linearity of the characteristic curve of the photographic film and especially its non-

linearity at the high intensity limit make it difficult for this technique to compare in accuracy with the photoelectric technique when determining the peak intensity of the line profile.

More modern techniques using image intensifiers or image orthicons (or combinations of both) are now being employed and provide some advantages and disadvantages, e.g., advantages such as photoelectric linearity, photographic spatial resolution, and time resolution with electrical shuttering; disadvantages such as high noise equivalent input (especially in time-resolved shutter mode) and fixed wavelength response due to the photocathode (can be extended into the ultraviolet with a scintillator).

c. Self-Absorption

Self-absorption as a competing effect to the broadening of a spectral line is often overlooked or mistreated. Many good experimental tests for optical thickness are available, such as increasing the plasma absorbing length or comparison of the peak intensity with a blackbody intensity. In the case of neutral non-hydrogenic atoms, the profile of a Stark broadened spectral line is usually represented by a dispersion or Lorentzian profile. In an attempt to provide experimental proof that self-absorption does not exist in the peak of experimentally observed line profiles, experimenters will fit a Lorentzian profile through their experimental results. It can be shown that this is very insensitive to the optical depth. Let us assume that there exists some optical depth, τ, in the plasma large enough so the spectral line intensity must be given by

$$I_\lambda = B_\lambda(T)(1 - e^{-\tau_\lambda}), \tag{8}$$

where

$$\tau_\lambda = \tau_{max} \left[1 - \left(\frac{\Delta\lambda}{\Delta\lambda_{1/2}^{true}} \right)^2 \right]^{-1}, \tag{9}$$

and the experimental points are fitted with a Lorentzian profile,

$$I_\lambda' = I_{peak} \left[1 - \left(\frac{\Delta\lambda}{\Delta\lambda_{1/2}^{fitted}} \right)^2 \right]^{-1}. \tag{10}$$

If both profiles are normalized so they match at the peaks and the halfwidths, then the plot shown in figure 2 of the ratio, $\Delta\lambda_{1/2}^{fitted}/\Delta\lambda_{1/2}^{true}$, versus τ_{max} can be obtained.

To demonstrate that erroneous halfwidths can result from large optical depths, a plot of the percent of deviation at a point on the profile where $I_\lambda/I_{peak} = 0.75$ has been made. This is shown in figure 3. It shows that for reasonably large τ's this deviation is quite small and could easily go undetected, especially in experiments where transient or nonhomogeneous sources are used or where a photographic technique is used to record the line shape, and the peak intensity is in the nonlinear part of the characteristic curve of the film. Take for example $\tau_{max} = 4$. The deviation is only 5 percent, but in figure 2 a $\tau_{max} = 4$ corresponds to a factor of 2 in the ratio of the Lorentzian fitted halfwidth to the true halfwidth.
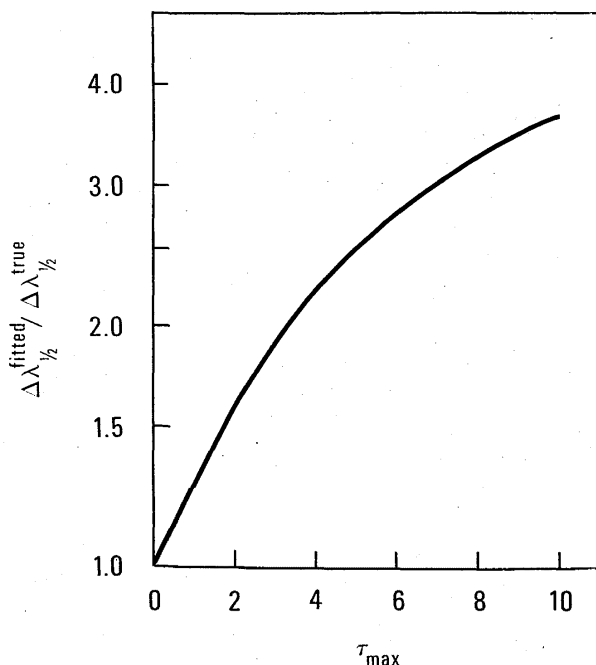
FIGURE 2. Ratio of $\Delta\lambda^{fitted}$ to $\Delta\lambda^{true}$ for a Lorentzian fitted, optically thick spectral line versus τ_{max}.
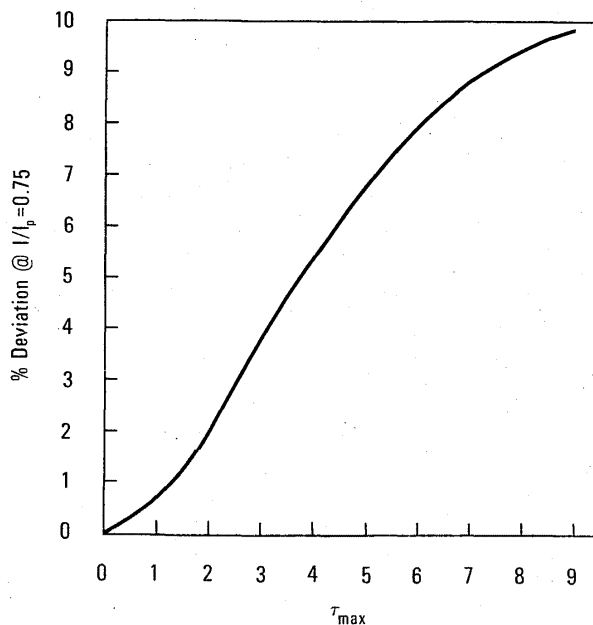
FIGURE 3. Percent deviation at $I_\lambda = 0.75\ I_{peak}$ of a Lorentzian fitted, optically thick spectral line versus τ_{max}.

d. Continuum Background

If the assignment of the continuous background underneath a broadened spectral line is not correctly made, an error in the halfwidth of the broadened line can result. As an example of this type of error, the correction to the halfwidth of a Lorentzian fitted experimental profile with an underlying continuum is discussed in detail in ref. [5], chap. 6. The basic result for a Lorentzian

fitted profile with an underlying continuum is that the true halfwidth $\Delta\lambda_{1/2}$ is given by

$$\frac{\Delta\lambda_{1/2}}{\Delta\lambda_{1/2}^{meas}} = \frac{\Delta\lambda_B}{\Delta\lambda_{1/2}^{meas}}\left[\left(\frac{\Delta\lambda_B}{\Delta\lambda_{1/2}^{meas}}\right)^2 - 2\right]^{-1/2}, \quad (11)$$

where $\Delta\lambda_B$ is the wavelength interval between the two points where the Lorentzian line wing intensity is taken to be zero, i.e., the width of the base line of the broadened spectral line, and where $\Delta\lambda_{1/2}^{meas}$ is the wavelength interval of the Lorentzian profile at the half intensity point using one-half the distance from the profile base line ($\Delta\lambda_B$) to the peak intensity as the half intensity point.

e. Impurity Lines and Blending

Impurity lines and the blending of spectral lines present additional sources of error in the determination of the true profile of broadened spectral lines. Obviously, if there exist other broadened lines in the near vicinity o: a Stark broadened line, their overlapping will contribute to the observed width in proportion to their intensities, widths, and closeness to the line under investigation. It is, therefore, very important to check available line lists to establish that no lines from other plasma species contribute to the Stark broadened line under investigation. Observations at differing plasma conditions, especially at differing electron densities, could also help to determine if impurity lines are present and will interfere. If blending, i.e., overlapping of line profiles, does occur and arises from the same plasma species, ionization stage, and Stark broadened states, so that the blended lines have the same amount of Stark broadening as the line under investigation, then the width of each of the lines can be determined by unfolding each profile using the appropriate theoretical profile function, e.g., Lorentzian or Voigt profiles (see section on competing effects).

f. Instrument Dispersion

In order to measure the width and shift of a spectral line, a dispersive instrument such as a monochromator, spectrometer, or interferometer must be used, and, therefore, an accurate measurement of the instrument dispersion is absolutely necessary. This is usually accomplished by using a spectral line source in the wavelength region of interest, whose line wavelengths are accurately known, to calibrate the instrument dispersion to within the accuracy required. Using a source whose line widths are much narrower than the instrument function (see next section), the instrumental widths can also be measured at the same time.

g. Instrumental Broadening

Because the dispersive instrument used in displaying the broadened profile has an instrumental width, this will contribute to the broadening of the profile and will result in erroneous line profiles if not properly taken into account. In the case of a monochromator or spectrometer, the instrumental function can usually be represented by a Gaussian profile (eq (14)). Deconvolution of the instru-

mental function represented, for example, by a Gaussian function and the Stark profile represented by a Lorentzian function has been documented, e.g., ref. [9], and the results of the deconvolution are represented in figure 4. In this graph, $\Delta\lambda^G_{1/2}$ represents the halfwidth of the Gaussian component, $\Delta\lambda^L_{1/2}$ represents the halfwidth of the Lorentzian component, and $\Delta\lambda_{1/2}$ represents the halfwidth of the measured profile.

In the case where the dispersive instrument is an interferometer, such as the Fabry-Perot, the instrumental function can be represented by an Airy function (e.g., see ref. [10]), and the deconvolution of this instrumental function from a Lorentzian and/or Gaussian has been documented [11].

h. Doppler Broadening

In section 2.2 a, eqs (3) and (4), the Doppler broadening contribution to a measured profile is given. This is deconvoluted from the measured profile in the same manner as when the instrumental function is represented by a Gaussian function, i.e., the graph of figure 4. For the case in which there are two or more competing mechanisms, such as instrumental and Doppler broadening that are represented by a Gaussian function, their deconvolution is attained by adding their widths in the following way to obtain a total Gaussian width to be deconvoluted:

$$\Delta\lambda^{\text{Total } G}_{1/2} = \sqrt{\left(\Delta\lambda^{\text{Inst.}}_{1/2}\right)^2 + \left(\Delta\lambda^{\text{Doppler}}_{1/2}\right)^2}. \quad (12)$$

On the other hand, two Lorentzian halfwidths add linearly, i.e.,

$$\Delta\lambda^{\text{Total } L}_{1/2} = \Delta\lambda^{L_1}_{1/2} + \Delta\lambda^{L_2}_{1/2}. \quad (13)$$

Other broadening mechanisms of some importance under certain experimental conditions such as van der Waals, resonance, Zeeman, and natural line broadening will not be discussed in detail but will be found, e.g., in ref. [3], chap. 4, and in ref. [12].

In all cases of competing broadening effects, the convolution of line shapes $I_1(\Delta\lambda)$ and $I_2(\Delta\lambda)$ is as follows:

$$I_{\text{meas}}(\Delta\lambda) = \int_{-\infty}^{+\infty} I_1(\Delta\lambda - \Delta\lambda') \, I_2(\Delta\lambda') \, d(\Delta\lambda'). \quad (14)$$

The example of I_1 equaling a Gaussian function and I_2 equaling a Lorentzian shape is the case presented in figure 4.

3. Review

The elements presented in the data tables are listed in alphabetical order. In keeping with the custom commonly employed in this field, energies and frequencies are often expressed in wavenumber (cm^{-1}) equivalents, as shown in the headings for each element. Associated with each element is (a) a brief introduction describing
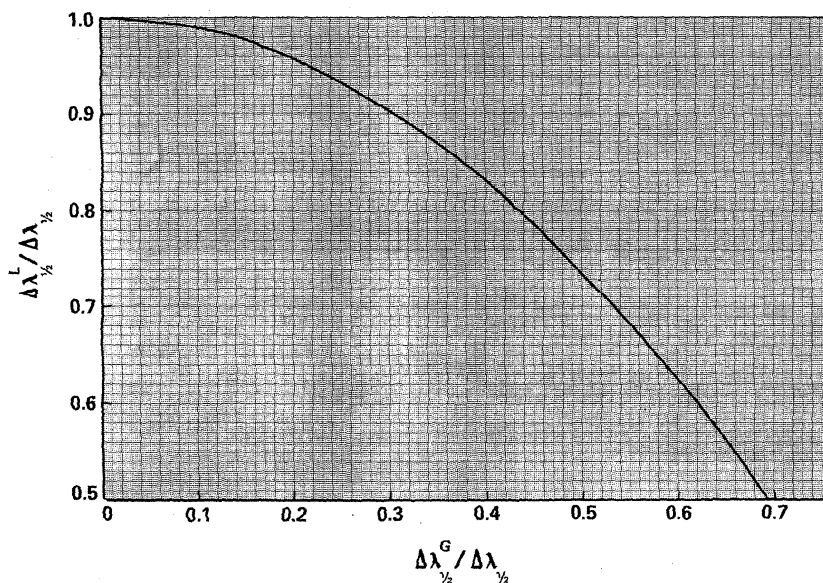

FIGURE 4. Deconvolution results of Lorentzian and Gaussian functions.

characteristics of the experiments including normalization values, references, and when more than 15 transitions are listed, a finding list is included, (b) a table giving a cursory description of important experimental quantities such as sources and method of electron density and temperature measurements, and finally (c) a table including all of the compiled results. In this compilation table the transition array is listed first and the transition (multiplet) is listed next with the multiplet number given by ref. [13] and the coupling scheme (L–S or j–l) according to [13–15]. The wavelength (Å) is listed in the next column. The temperature and electron density columns list the experimental conditions. If single values are given, then the experiment was done either at one set of conditions or these values are normalized and are so noted in the introduction of each element. This same single entry description is also valid for the halfwidth (w_m), the experimental-to-theoretical halfwidth ratio (w_m/w_{th}), the shift (d_m), and the experimental-to-theoretical shift ratio (d_m/d_{th}). The reference column (Ref.) lists the number associated with references listed in the introduction of each element. The accuracy column lists letters A through D which correspond to the total uncertainty estimates listed for each transition. This correspondence is given in table 2. These uncertainties are arrived at from the uncertainties listed in the particular references (if any), by comparison of experiments for the same transition, by observing any systematic deviation of halfwidths within the same multiplet for each experiment, the recording technique, experimental checks for optical depths, and the normalization of data due to source transiency and inhomogeneities.

In the data tables, we have chosen to give the end points of measured-to-theoretical widths and shift ratios when available for the range of electron density given in the experiment. This will allow the reader to tell at a glance something about the agreement between experiment and theory over the entire range. A great number of experimental results were normalized to a single electron density-temperature, but since the normalized electron density is near to the experimental value, they should provide reliable comparisons.

The total theoretical width, w_{th}, and the total theoretical shift, d_{th}, were obtained using the approximate formula of ref. [1], eqs. (226) and (227), i.e.,

$$w_{th} \approx 2[1 + 1.75 \times 10^{-4} N_e^{1/4} A$$
$$\times (1 - 0.068 N_e^{1/6} T^{-1/2})]10^{-16} w N_e , \quad (15)$$

TABLE 2. Accuracy and uncertainty correspondence

Accuracy	Uncertainty
A	$\leq 15\%$
B	$\leq 30\%$
C	$\leq 50\%$
D	$> 50\%$

$$d_{th} \approx [d \pm 2.0 \times 10^{-4} N_e^{1/4} A$$
$$\times w(1 - 0.068 N_e^{1/6} T^{-1/2})]10^{-16} N_e , \quad (16)$$

where w and d are the width and shift, respectively, A is the ion broadening parameter, all given in the tables of ref. [1] at $N_e = 10^{16}$, and N_e and T are the electron density (cm^{-3}) and temperature (K), at which w_{th} and d_{th} are to be given. There are certain restrictions on the applicability of eqs. (15) and (16) and they are:

(a) $B = 8.99 \times 10^{-2} N_e^{1/6} T^{-1/2} \lesssim 0.8$

(b) $0.05 \lesssim A \lesssim 0.5$.

Other considerations, such as Debye shielding, affecting line shapes, widths, and shifts are covered in ref. [1] and ref. [5], chap. 6.

It should be noted also that some spectral lines do not have symmetric Lorentzian shapes, e.g., due to a large ionic contribution. Under these circumstances, a measure of the asymmetry as well as the total width should be included in the experimental results, e.g., a ratio of the blue-to-red half-halfwidths as measured from the peak intensity wavelength.

4. Discussion of Results

There were three points that stood out in the compilation of the data. They were (a) systematic trends of experimental halfwidths within a multiplet of a particular element as a function of line intensity for certain experiments, (b) the systematic trend of the experimental-to-theoretical halfwidth ratio as a function of temperature, and (c) the systematic trend of the experimental-to-theoretical halfwidth ratio as a function of upper principal quantum number for the alkali metals.

An example of the systematic trend mentioned in (a) is seen in the case of Zn I where multiplets 2, 4, and 5 uv exhibit the systematic trend of increasing experimental halfwidth as a function of increasing intensity within the multiplet, but for the higher excitation energy and lower intensities of multiplet 5 [13], this trend is not observed. On the other hand, theory [1] predicts the same widths for lines within a multiplet whose wavelengths are nearly the same (however, no calculations exist for Zn I in ref. [1]). Possible explanations for this systematic trend in some experiments may be the breakdown of this general theoretical rule or the possibility of optical depth problems in the peak intensities of the observed lines. This latter possibility has the correct systematic dependence of experimental halfwidth on intensity, whereas the breakdown of the theoretical rule could be a random function of the intensity. Another example of this trend is demonstrated in Cl I multiplet 2 where there exist two experiments and a theoretical comparison. The results of the experiment of ref. [1] in the chlorine table show the systematic trend as a function of intensity where the more intense 8248.2 Å and 8212.0 Å lines ($\sim$ equal intensity [14]) have broader widths when

compared with the less intense 8194.4 Å line ($\sim$40 percent as intense [14]). Contrast this to the experiment of ref. [2] of the chlorine table, in which all three of these lines have approximately the same widths. It appears that optical depth is a significant contributing factor to explain this systematic trend for this multiplet in chlorine for ref. [1] of the chlorine table.

The second systematic trend mentioned in (b) is the tendency of the measured-to-theoretical halfwidth ratio to decrease as the temperature increases, and this was found to occur very often when there existed a range of experimental conditions. This is best demonstrated by observing the N I multiplet 9 where the experimental temperature range was 12,000 K. A plot of the experimental halfwidth versus temperature is presented in figure 5, and even though there exists some experimental scatter, the tendency of the experimental width to become smaller than the theoretical width [1] as the temperature increases is quite evident. Because of the nonconstant deviation of the experimental-to-theoretical ratio, it is difficult to recommend certain experimentally determined halfwidths as possible standards for use at experimental conditions outside of the range of the original measurements. A possible reason for this discrepancy between theory and experiment may be due to a systematic tendency in the experimental electron density-temperature determination of the plasma source. This, however, seems unlikely since this trend occurs no matter what method is used in determining the experimental conditions and no matter what source is used. This discrepancy may also be due to an incorrect theoretical dependence of the Stark width as a function of temperature.

The systematic trend mentioned in (c) is most obvious in the case of Cs I. In figure 6, the measured-to-theoretical width ratio of three series of Cs I presented in the data table are plotted as a function of upper principal quantum number. For the sharp and diffuse series, it was found that this trend was also a function of the particular L and J quantum numbers. This same effect is observed in the shifts of Cs I lines in ref. [16]. Lithium and sodium

also exhibit this tendency, but there are reliable data for only two upper principal quantum numbers. A possible explanation for this phenomenon is the breakdown of the various approximations included in the theory of Stark broadening [1]. The two approximations that are violated for certain quantum numbers under the experimental conditions described in Cs I are the omission of Debye shielding (this correction is not included in the calculations of [1]) and the breakdown of the isolated line approximation. They are simply stated as:

Debye Shielding: $\bar{\lambda}_{\alpha\alpha'} \gg \bar{\lambda}_{\text{plasma freq.}}$

Isolated Line: $\bar{\lambda}_{\alpha\alpha'} \gg \bar{\lambda}_{\text{width}}$,

where $\bar{\lambda}_{\alpha\alpha'}$ is the wave number (cm^{-1}) associated with the perturbed level α and the next interacting level α', $\bar{\lambda}_{\text{plasma freq.}}$ is the wave number (cm^{-1}) associated with the plasma frequency given by eq. (17),

$$\bar{\lambda}_{\text{plasma freq.}} = \left(\frac{e^2}{\pi m c^2} N_e\right)^{1/2} = 2.995 \times 10^{-7} N_e^{1/2}, \quad (17)$$

and $\bar{\lambda}_{\text{width}}$ is the wave number (cm^{-1}) associated with the halfwidth of the spectral line and is given in terms of the broadened line's total halfwidth, $\Delta\lambda_{1/2}$, and central wavelength, λ_0, by,

$$\bar{\lambda}_{\text{width}} = \Delta\lambda_{1/2}/\lambda_0^2. \quad (18)$$

The progressive breakdown of these two approximations for Cs I is demonstrated in table 3 as the upper principal quantum number increases.

5. Conclusions

In general the agreement between experiments and between experiment and theory is quite good. There are some points, however, that should be emphasized in making these comparisons. The first point is that because
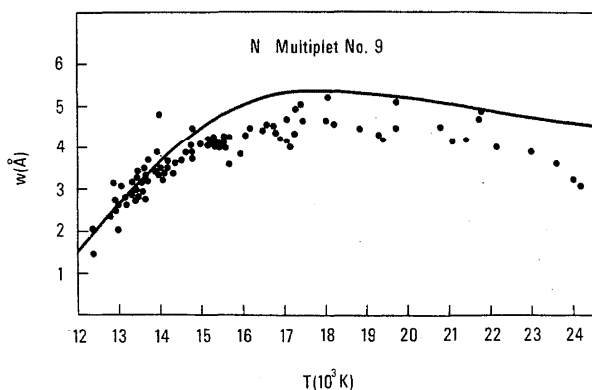
FIGURE 5. Stark width of N I multiplet 9 versus temperature. "." the experimental points of ref. [5] of the nitrogen table and "—" the theoretical results of ref. [1].
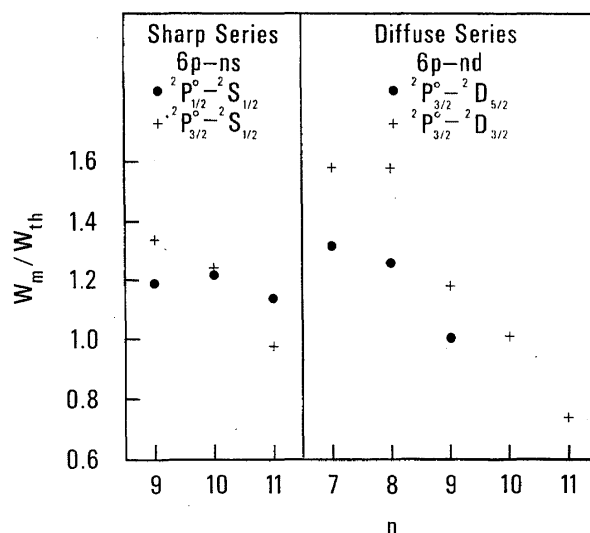
FIGURE 6. w_m/w_{th} ratio versus upper principal quantum number for three spectral series in Cs I of ref. [1] of Cs table.

TABLE 3. Comparisons between $\bar{\lambda}_{\alpha\alpha'}$ and λ for the Debye shielding and isolated line approximations for an experiment in Cs I from ref. [1] of Cs table

$\lambda(\text{Å})$	α Design.	α' Design.	$\bar{\lambda}_{\alpha\alpha'}$ (cm^{-1})	(Debye Shielding) $\lambda_{\text{Plasma Freq.}}$ (cm^{-1})	(Isolated Line) $\bar{\lambda}_{\text{width}}$ (cm^{-1})	w_m/w_{th}
6973.3	$7d\,^2D_{5/2}$	$8p\,^2P^\circ_{3/2}$	277.1	12	1.6	1.58
6213.1	$8d$	$9p$	141.0	12	3.9	1.58
5845.1	$9d$	$10p$	82.1	12	8.2	1.18
5635.2	$10d$	$11p$	52.1	11	12.3	1.01
5503.9	$11d$	$12p$	35.2	11	16.8	0.74

experiment and theory have a tendency to disagree more and more the larger the temperature variation, the extension of the compiled experimental results outside the experimental temperature range should be done with extreme caution. The second point is that an extra degree of confidence should be placed in those experiments in which care has been taken to investigate (and communicate) all other broadening and competing mechanisms and those that have independent experimental comparisons which agree, especially using different plasma sources. A third point is related to the first two and that is to suggest that investigators should choose their experiments so that they test points like the theoretical temperature variation and, most important, to make more than one independent determination of the electron density and to check for other broadening and competing mechanisms, such as Doppler broadening, instrumental broadening, and optical depth.

It cannot be overemphasized that actual experimental results of N_e and T should be stated in each publication and should not be just normalized values.

6. References for Sections 1-5

[1] Griem, H. R., Spectral Line Broadening by Plasmas, Academic Press, (1974).

[2] Fuhr, J. R., Wiese, W. L., and Roszman, L. J., Bibliography on Atomic Line Shapes and Shifts (1889 through March 1972), Natl. Bur. Stand. (U.S.), Spec. Publ. 366, (1972) and Fuhr, J. R., Roszman, L. J., and Wiese, W. L., Bibliography on Atomic Line Shapes and Shifts (April 1972 through June

1973), Natl. Bur. Stand. (U.S.), Spec. Publ. 366, Suppl. 1, (1974).

[3] Griem, H. R., Plasma Spectroscopy, McGraw-Hill, Inc., New York, (1964).

[4] Plasma Diagnostics, Lochte-Holtgreven, W., Editor, North-Holland Publishing Co., Amsterdam, (1968).

[5] Plasma Diagnostic Techniques, Huddlestone, R. H. and Leonard, S. L., Editors, Academic Press, New York, (1965).

[6] Wiese, W. L., Kelleher, D. E., and Paquette, D. R., Phys. Rev. A 6, 1132 (1972).

[7] Roberts, J. R., and Voigt, P. A., J. Res. Natl. Bur. Stand. (U.S.) A 75, 291 (1971).

[8] Eckerle, K. L., and McWhirter, R. W. P., Phys. Fluids 9, 81 (1966).

[9] Davies, J. T., and Vaughan, J. M., Astrophys. J. 137, 1302 (1963).

[10] Cooper, J., and Grieg, J. R., J. Sci. Instrum. 40, 433 (1963).

[11] Larson, H. P., and Andrew, K. L., Appl. Opt. 6, 1701 (1967).

[12] Aller, L. H., Astrophysics, The Ronald Press Co., New York, (1963).

[13] Moore, C. E., A Multiplet Table of Astrophysical Interest, Natl. Bur. Stand. (U.S.), Tech. Note 36, (1959) and An Ultraviolet Multiplet Table, Natl. Bur. Stand. (U.S.), Circ. 488, sections 1–5, (1950).

[14] Wiese, W. L., Smith, M. W., and Glennon, B. M., Atomic Transition Probabilities (H through Ne), Vol. I, Natl. Stand. Ref. Data Ser. Natl. Bur. Stand. (U.S.) 4, (1966) and Wiese, W. L., Smith, M. W., and Miles, B. M., Atomic Transition Probabilities (Na through Ca), Vol. II, Nat. Stand. Ref. Data Ser. Natl. Bur. Stand. (U.S.) 22, (1969).

[15] Striganov, A. R. and Sventitskii, N. S., Tables of Spectral Lines of Neutral and Ionized Atoms, IFI/Plenum, New York-Washington, (1968).

[16] Majkowski, R. F., and Donohue, R. J., Phys. Rev. 173, 177 (1968).

7. Data Tables

7.1. Argon

Ar I

Ground State	$1s^2 2s^2 2p^6 3s^2 3p^6$ $^1S_0$
Ionization Potential	15.755 eV = 127109.9 cm^{-1}

Wavelength	No.	Wavelength	No.	Wavelength	No.	Wavelength	No.
1048.2	2	5151.4	94	6098.8	103	7272.9	16
1066.7	1	5162.3	95	6105.6	84	7384.0	15
3606.5	45	5187.7	73	6145.4	86	7503.9	20
3947.5	25	5221.3	104	6296.9	87	7514.6	14
3949.0	26	5252.8	105	6307.7	81	7635.1	10
4044.4	32	5254.5	98	6364.9	78	7948.2	19
4046.0	33	5421.4	106	6369.6	80	10470.1	18
4054.5	31	5451.6	100	6384.7	89	10673.6	61
4158.6	24	5495.9	96	6416.3	88	12356.8	5
4164.2	23	5506.1	97	6431.6	92	12456.1	64
4181.9	36	5525.0	75	6538.1	54	12487.6	62
4191.0	35	5550.7	72	6604.0	55	12733.6	63
4198.3	30	5559.7	99	6660.7	93	12933.3	67
4200.7	22	5572.5	77	6664.0	56	13008.5	68
4251.2	21	5606.7	71	6677.3	17	13214.7	46
4259.4	44	5650.7	70	6698.9	58	13231.4	65
4266.3	29	5739.5	79	6719.2	83	13367.1	69
4272.2	28	5834.3	82	6752.8	50	13406.6	3
4300.1	27	5860.3	91	6766.6	60	13910.8	4
4333.6	42	5882.6	90	6827.2	85	14249.9	66
4335.3	43	5888.6	101	6871.3	49	14257.4	8
4345.2	41	5912.1	53	6879.6	57	14596.3	9
4510.7	40	5928.8	102	6937.7	48	14634.1	7
4522.3	34	6032.1	74	6951.5	59	14649.9	6
4596.1	39	6043.2	76	6965.4	13	20986.1	47
4628.4	38	6052.7	51	7067.2	12		
4702.3	37	6059.4	52	7147.0	11		

An extensive number of experimental Stark broadening data exist for neutral argon lines from which 17 papers were selected [1-17]. Most of the results were obtained in wall-stabilized arcs [1, 2, 7, 9, 13-16] and plasma jets [3, 4, 17], but other plasma sources were also used.

The results show that in most cases theory predicts larger widths than are experimentally measured. Nevertheless, the agreement in general is within the combined experimental and theoretical uncertainties. In a few cases the agreement with the theory is poor (more than ±50 percent). These are widths of infrared lines [6]. Measured shifts also agree with the theory. The exceptions are data for some infrared lines [6] and also the 6296.9 Å and 7968.2 Å lines [9], where the theory predicts shifts in the opposite direction.

The graphical results of ref. [2] are averaged values obtained by drawing a best fit curve through the experimental data points. In ref. [15] the extreme values adopted for this table are averaged values of two sets of data obtained by different experimental techniques. The

7948.2 Å line of ref. [3] is reported to be asymmetric, as well as having a shift in a direction opposite to theory. The results of refs. [10] and [17] are given normalized to $N_e = 1.0 \times 10^{16}$ cm^{-3} and ref. [11] to $N_e = 1.0 \times 10^{17}$ cm^{-3}.

References

[1] Gericke, W. E., Z. Astrophys. 53, 68 (1961).
[2] Popenoe, C. H. and Shumaker, J. D. Jr., J. Res. Nat. Bur. Stand. Sect. A 69, 495 (1965).
[3] Murakawa, K., Yamamoto, M. and Hashimoto, S., Proc. VIIth Intl. Conf. Phen. Ion. Gases, Vol. II, p. 594, Gradevinska Knjiga Publishing House, Belgrade, (1966).
[4] Chapelle, J., Cabonne, Sy, A., Cabannes, F., and Blandin, J., J.Q.S.R.T. 8, 1201, (1967); C.R.H. Acad. Sci., Ser. B, 264, 853 (1967).
[5] Evans, D., and Tankin, R. S., Phys. Fluids 10, 1137 (1967).
[6] Assous, R., J. Phys. (Paris) 29, 877 (1968).
[7] Schulz, P., and Wende, B., Z. Phys. 208, 116 (1968).
[8] Bober, L., and Tankin, R. S., J.Q.S.R.T. 9, 855 (1969).
[9] Bues, I., Haag, T., and Richter, J., Astron. Astrophys. 2, 249 (1969).

[10] Powell, W. R., Ph.D. Thesis, The Johns Hopkins University (1966).

[11] Miller, M. H., and Bengtson, R. D., Phys. Rev. A 1, 983 (1970).

[12] Moo-Young, C. A., Grieg, J. R., and Griem, H. R., Phys. Rev. A 2, 1617 (1970).

[13] Morris, J. C., and Morris, R. U., Aerospace Research Laboratories, Report No. ARL 70 0038.

[14] Queffelec, J. L., and Girault, M., Rev. Phys. Appl. 6, 401 (1971).

[15] Tonejc, A., J.Q.S.R.T. 12, 1713 (1972).

[16] Tonejc, A. M., Acinger, K., and Vujnovic, V., J.Q.S.R.T. 12, 1305 (1972).

[17] Ranson, P., and Chapelle, J., J.Q.S.R.T. 14, 1 (1974).

[18] Helbig, V., private communication (1974).

[19] Griem, H. R., Phys. Rev. 128, 515 (1962).

Key data on experiments

Ref.	Plasma source	Method of measurement		Remarks
		Electron density	Temperature	
[1]	Wall-stabilized arc	Plasma composition data	Absolute intensity of Ar II 4348.1 Å line	Experimental data for T & N_e are corrected by ref. [19] and the corrected values are given in the data table
[2]	Wall-stabilized arc	H_β	Plasma composition data	
[3]	Plasma jet	Plasma composition data	Absolute intensity of Ar I 7948.2 Å line	
[4]	Plasma jet	Plasma composition data	Absolute intensity of Ar I 4158.6 Å line and intensity of continuum	
[5]	High current, free-burning arc	Plasma composition data	Fowler-Milne method and absolute Ar I line intensities	
[6]	Radio-frequency discharge	H_β	Plasma composition data	
[7]	Wall-stabilized arc	Plasma composition data	Absolute intensities of Ar I and Ar II lines	
[8]	High current, free-burning arc	Plasma composition data	Fowler-Milne method and absolute intensities of Ar I lines	
[9]	Wall-stabilized arc	H_β	Generalized Fowler-Milne method; absolute intensity of Ar II 6806.0 Å line, absolute intensity of continuum at 3960 Å	
[10]	Electric T tube	H_β, H_α	Absolute line intensities	
[11]	Gas driven shock tube	H_β	Absolute line intensity, line reversal technique	
[12]	Electric T tube	H_β	Absolute and relative line intensities	Measurements of wings of optically thick lines
[13]	Wall-stabilized-pulsed arc	H_β	Absolute line intensities	
[14]	Wall-stabilized arc	H_β	Plasma composition data	
[15]	Wall-stabilized arc	H_β	Absolute intensity of Ar II 4300.6 Å line	
[16]	Wall-stabilized arc	H_β	Absolute intensity of Ar II 4300.6 Å line	
[17]	Plasma jet	H_β	Boltzmann plot of intensities of hydrogen lines	
[18]	Wall-stabilized arc	H_β	Plasma composition data	

No.	Transition array	Transition jl-coupling (Multiplet)	Wavelength (Å)	Temperature (K)	Electron density (cm⁻³)	w_m(Å)	w_m/w_{th}	d_m(Å)	d_m/d_{th}	Acc.	Ref.
1.	$3p$–$4s$	^1S–[1 1/2]° (1 uv)	1066.7	15000	1.4×10^{17}	13.28×10^{-3}	0.76			D	[12]
2.	$3p$–$4s'$	^1S–[1/2]° (2 uv)	1048.2	15000	1.4×10^{17}	14.28×10^{-3}	0.80			D	[12]
3.	$3d$–$4f$	[3 1/2]°–[4 1/2]	13406.6	10050	1.9×10^{16}	6.3	1.20	−1.3	9.34	C	[6]
4.	$3d$–$4f$	[3 1/2]°–[4 1/2]	13910.8	10050	1.9×10^{16}	6.3		−3.0		C	[6]
5.	$3d$–$4f$	[1 1/2]°–[2 1/2]	12356.8	10050	1.9×10^{16}	5.9				C	[6]
6.	$3d$–$4f$	[2 1/2]°–[3 1/2]	14649.9	10050	1.9×10^{16}	8.0		−2.8		C	[6]
7.	$3d'$–$4f'$	[2 1/2]°–[3 1/2]	14634.1	10050	1.9×10^{16}	6.8	0.90	−3.0	0.54	C	[6]
8.	$3d'$–$4f'$	[2 1/2]°–[3 1/2]	14257.4	10050	1.9×10^{16}	7.5				C	[6]
9.	$3d'$–$4f'$	[1 1/2]°–[2 1/2]	14596.3	10050	1.9×10^{16}	8.2		−2.0		C	[6]
10.	$4s$–$4p$	[1 1/2]°–[1 1/2] (1)	7635.1	13800 10000–22000 10300–11500	1.45×10^{17} $(0.2–1.9) \times 10^{17}$ $(2.0–5.0) \times 10^{16}$	1.46 0.4–1.8 0.2–0.5		0.17–0.85		C C C	[4] [8] [15]
11.	$4s$–$4p'$	[1 1/2]°–[1 1/2] (1)	7147.0	10300–12500	$(2.0–8.8) \times 10^{16}$	0.16–0.70				B	[16]
12.	$4s$–$4p'$	[1 1/2]°–[1 1/2] (1)	7067.2	13800 10300–12350	1.45×10^{17} $(2.0–8.0) \times 10^{16}$	0.75 0.14–0.65				C B	[4] [16]
13.	$4s$–$4p'$	[1 1/2]°–[1/2] (1)	6965.4	9700–11800 13800 10000–20000 9700–12250	$(1,2–6.0) \times 10^{16}$ 1.45×10^{17} $(0.48–1.96) \times 10^{17}$ $(1.2–7.7) \times 10^{16}$	0.14–0.63 0.30 0.40–1.40 0.08–0.66		0.05–0.23 0.17–0.67		B C C B	[2] [4] [5] [16]
14.	$4s$–$4p$	[1 1/2]°–[1/2]	7514.6	10300–11500	$(2.0–5.0) \times 10^{16}$	0.23–0.53				C	[15]
15.	$4s$–$4p'$	[1 1/2]°–[1 1/2]	7384.0	10300–11500	$(2.0–5.0) \times 10^{16}$	0.18–0.42				D	[15]
16.	$4s$–$4p'$	[1 1/2]°–[1/2]	7272.9	10300–12500	$(2.0–8.5) \times 10^{16}$	0.18–0.80				B	[16]
17.	$4s$–$4p'$	[1 1/2]°–[1/2]	6677.3	11400–12700	$(4.79–.4) \times 10^{16}$	0.40–0.82		0.31–0.54		B	[9]

J. Phys. Chem. Ref. Data, Vol. 5, No. 2, 1976

222

N. KONJEVIC AND J. R. ROBERTS

Numerical results for ArI— Continued

No.	Transition array	Transition j-l coupling (Multiplet)	Wavelength (Å)	Temperature (K)	Electron density (cm⁻³)	w_m(Å)	w_m/w_{th}	d_m(Å)	d_m/d_{th}	Acc.	Ref.
18.	4s'–4p	[1/2]°–[1/2] (6)	10470.1	10050	1.9×10^{16}			-0.5		C	[6]
				14500–15600	$(1.0-1.8) \times 10^{17}$	0.81–1.30	0.70–0.60	$(-1.20)-(-1.83)$	$(-3.18)^a-(-2.70)^a$	C	[3]
19.	4s'–4p'	[1/2]°–[1 1/2] (6)	7948.2	13800	1.45×10^{17}	1.29	0.85			C	[4]
				10200–11500	$(1.9-5.1) \times 10^{16}$	0.20–0.53	1.04–1.02			C	[15]
20.	4s'–4p'	[1/2]°–[1/2] (8)	7503.9	13800	1.45×10^{17}	1.69				C	[4]
				10300–11500	$(2.0-5.0) \times 10^{16}$	0.28–0.60				C	[15]
21.	4s–5p	[1 1/2]°–[1/2] (2)	4251.2	11400	4.6×10^{16}	0.7				C	[1]
				9700–12350	$(1.2-7.3) \times 10^{16}$	0.2–1.14		0.11–0.65		B	[9]
22.	4s–5p	[1 1/2]°–[2 1/2] (2)	4200.7	13800	1.45×10^{17}	3.24	0.90	0.80	0.50	C	[4]
				9750–12700	$(1.2-9.4) \times 10^{16}$	0.19–1.55	0.74–0.70	0.12–0.88	0.95–0.85	B	[9]
				13500	1.28×10^{17}			1.20	0.87	C	[13]
				11400	4.6×10^{16}	1.0	0.96	0.44	0.88	C	[1]
				9720–12610	$(0.17-0.92) \times 10^{17}$	0.33–1.80	0.90–0.82	0.14–0.85	0.78–0.84	B	[19]
23.	4s–5p	[1 1/2]°–[1 1/2] (2)	4164.2	13800	1.45×10^{17}	3.62				C	[4]
				9750–12700	$(1.2-9.4) \times 10^{16}$	0.19–1.71		0.11–0.79		B	[9]
				14000	1.0×10^{16}	0.181		0.10		C	[10]
				11400	4.6×10^{16}	1.0		0.42		C	[1]
				13800	1.45×10^{17}	3.32		0.75		C	[4]
24.	4s–5p	[1 1/2]°–[1 1/2] (2)	4158.6	9750–12700	$(1.2-9.4) \times 10^{16}$	0.20–1.73		0.13–0.94		B	[9]
				14000	1.0×10^{16}	0.183		0.099		C	[10]
				13500	1.28×10^{17}			1.42		C	[13]
				11400	4.6×10^{16}	1.1		0.50		C	[1]
				9720–14830	$(0.17-1.80) \times 10^{17}$	0.36–3.51		0.16–1.72		B	[19]
25.	4s–5p'	[1 1/2]°–[1 1/2] (2)	3947.5	9750–11450	$(1.2-4.7) \times 10^{16}$	0.23–0.76		0.10–0.39		B	[9]
26.	4s–5p'	[1 1/2]°–[1/2] (2)	3949.0	13800	1.45×10^{17}	3.1		0.98		C	[4]
				9750–12700	$(1.2-9.4) \times 10^{16}$	0.25–1.96		0.12–0.84		B	[9]
				9950–12800	$(1.5-10.0) \times 10^{16}$	0.32–2.04		0.16–1.06		B	[2]
				13800	1.45×10^{17}	3.47		0.95		C	[4]
				9650–12500	$(1.1-8.6) \times 10^{16}$	0.21–1.62				B	[7]

No.	Transition array	Transition j-l coupling (Multiplet)	Wavelength (Å)	Temperature (K)	Electron density (cm^{-3})	w_m(Å)	w_m/w_{th}	d_m(Å)	d_m/d_{th}	Acc.	Ref.
27	4s–5p	[1 1/2]°–[2 1/2] (4)	4300.1	9750–12700	$(1.2–9.4) \times 10^{16}$	0.19–1.69		0.12–0.89		B	[9]
				14000	1.0×10^{16}	0.184		0.097		C	[10]
				13500	1.28×10^{17}			1.31		C	[13]
				9600–11800	$(1.1–5.9) \times 10^{16}$	0.25–0.75		0.10–0.73		B	[14]
				11400	4.6×10^{16}	1.0		0.49		C	[1]
				9720–13500	$(0.17–1.32) \times 10^{17}$	0.32–2.53		0.13–1.15		B	[19]
28	4s–5p	[1 1/2]°–[1 1/2] (4)	4272.2	13800	1.45×10^{17}	3.15	0.93	1.02	0.71	C	[4]
				9750–12700	$(1.2–9.4) \times 10^{16}$	0.20–1.69	0.79–0.80	0.12–0.89	1.02–0.93	B	[9]
				13500	1.28×10^{17}			1.21	0.94	C	[13]
				11400	4.6×10^{16}	1.0	0.98	0.44	0.96	C	[1]
				9750–12700	$(1.2–9.4) \times 10^{16}$	0.21–1.91		0.15–0.96		B	[9]
29	4s–5p	[1 1/2]°–[1 1/2] (4)	4266.3	14000	1.0×10^{16}	0.179		0.090		C	[10]
				13500	1.28×10^{17}			1.29		C	[13]
				11400	4.6×10^{16}	1.1		0.50		C	[1]
30	4s–5p	[1 1/2]°[1/2] (4)	4198.3	9750–12400	$(1.2–7.3) \times 10^{16}$	0.22–1.20	0.56–0.46	0.18–0.95	0.88–0.74	B	[9]
				14000	1.0×10^{16}	1.0	0.65	0.54	0.68	C	[1]
31	4s–5p'	[1 1/2]°–[1 1/2]	4054.5	9750–11450	$(1.2–4.7) \times 10^{16}$	0.24–0.84		0.12–0.42		B	[9]
32	4s–5p'	[1 1/2]°–[1 1/2] (4)	4044.4	13800	1.45×10^{17}	2.72		1.20		C	[4]
				9650–12500	$(1.1–8.6) \times 10^{16}$	0.18–1.33				B	[7]
				9750–12700	$(1.24–9.4) \times 10^{16}$	0.20–1.66		0.11–0.81		B	[9]
				13500	$(1.28) \times 10^{17}$			1.24		C	[13]
33	4s–5p'	[1 1/2]°–[1/2]	4046.0	9750–10500	$(1.2–2.47) \times 10^{16}$	0.28–0.50		0.13–0.28		B	[9]
34	4s'–5p	[1/2]°–[1/2] (7)	4522.3	9750–12700	$(1.2–9.4) \times 10^{16}$	0.22–2.00		0.10–0.89		B	[9]
35	4s'–5p'	[1/2]°–[1 1/2] (7)	4191.0	13800	1.45×10^{17}	2.72		1.05		C	[4]
36	4s'–5p'	[1/2]°–[1/2] (7)	4181.9	13800	1.45×10^{17}	3.20		1.06		C	[7]
				9650–12500	$(1.1–8.6) \times 10^{16}$	0.27–2.00				B	[4]
				9750–12700	$(1.2–9.4) \times 10^{16}$	0.23–2.00		0.15–1.04		B	[9]
				13500	1.28×10^{17}			1.43		C	[1]
				11400	4.6×10^{17}	1.2		0.50		C	[9]
37	4s'–5p	[1/2]°–[1/2] (9)	4702.3	9750–12700	$(1.2–9.4) \times 10^{16}$	0.23–1.89		0.12–0.92		B	[13]

N. KONJEVIC AND J. R. ROBERTS

No.	Transition array	Transition j-l coupling (Multiplet)	Wavelength (Å)	Temperature (K)	Electron density (cm⁻³)	w_m(Å)	w_m/w_{th}	d_m(Å)	d_m/d_{th}	Acc.	Ref.
38.	4s'-5p	[1/2]°-[1 1/2] (9)	4628.4	9750-12400	$(1.2-7.3) \times 10^{16}$	0.25-1.65		0.14-0.88		B	[9]
39.	4s'-5p	[1/2]°-[1 1/2] (9)	4596.1	9750-12700	$(1.2-9.4) \times 10^{16}$	0.24-2.00		0.12-1.01		B	[9]
40.	4s'-5p	[1/2]°-[1/2] (9)	4510.7	13800	1.45×10^{17}	3.85	0.67			C	[4]
				9750-12700	$(1.2-9.4) \times 10^{16}$	0.25-2.18	0.55-0.57	0.16-1.36	0.68-0.71	B	[9]
41.	4s'-5p'	[1/2]°-[1 1/2] (9)	4345.2	9750-12400	$(1.2-7.3) \times 10^{16}$	0.21-1.37		0.13-0.74		B	[9]
				11400	4.6×10^{16}	1.1		0.50		C	[1]
42.	4s'-5p'	[1/2]°-[1 1/2] (9)	4333.6	13800	1.45×10^{17}	3.20		0.95		C	[4]
				9750-12700	$(1.2-9.4) \times 10^{16}$	0.21-1.78		0.13-1.03		B	[9]
				11400	4.6×10^{16}	1.1		0.54		C	[1]
43.	4s'-5p'	[1/2]°-[1/2] (9)	4335.3	9750-11450	$(1.2-4.7) \times 10^{16}$	0.28-1.18		0.16-0.53		B	[9]
				11400	4.6×10^{16}	1.5		0.55		C	[1]
				13800	1.45×10^{17}	3.78	0.81	0.94	0.42	C	[4]
				9550-12100	$(1.0-7.0) \times 10^{16}$	0.20-1.60	0.72-0.74			B	[7]
44.	4s'-5p'	[1/2]°-[1/2] (9)	4259.4	9750-12700	$(1.2-9.4) \times 10^{16}$	0.23-1.97	0.68-0.70	0.14-0.05	0.82-0.73	B	[9]
				14000	1.0×10^{16}	0.187	0.60	0.05	0.34	C	[10]
				13500	1.28×10^{17}			1.67	0.85	C	[13]
				11400	4.6×10^{16}	1.2	0.87	0.56	0.81	C	[1]
45.	4s-6p	[1 1/2]°-[1/2] (5)	3606.5	9650-12500	$(1.1-8.6) \times 10^{16}$	0.45-5.0	0.46-0.59			B	[7]
46.	4p-3d	[1/2]-[1/2]°	13214.7	10050	1.9×10^{16}			-1.6		C	[6]
47.	4p-3d	[1/2]-[1/2]°	20986.1	10050	1.9×10^{16}	3.9				C	[6]
48.	4p-4d	[1/2]-[1/2]°	6937.7	9750-11450	$(1.2-4.7) \times 10^{16}$	0.82-3.21		(-0.10)-0.95		B	[9]
49.	4p-4d	[1/2]-[1/2]°	6871.3	9750-11450	$(1.2-4.7) \times 10^{16}$	0.81-3.11		0.48-1.04		B	[9]
50.	4p-4d	[1/2]-[1 1/2]°	6752.8	11000	1.0×10^{17}	9.4				C	[11]
				9750-11000	$(1.2-3.55) \times 10^{16}$	0.76-2.14		0.25-0.86		B	[9]
51.	4p-4d'	[1/2]-[1 1/2]°	6052.7	9100-11000	$(0.63-3.55) \times 10^{16}$	0.39-2.27		0.25-1.08		B	[9]
52.	4p-4d'	[1/2]-[1 1/2]°	6059.4	9110-11450	$(0.63-4.70) \times 10^{16}$	0.39-3.25		0.28-1.33		B	[9]

No.	Transition array	Transition j-l coupling (Multiplet)	Wavelength (Å)	Temperature (K)	Electron density (cm^{-3})	w_m(Å)	w_m/w_{th}	d_m(Å)	d_m/d_{th}	Acc.	Ref.
53.	$4p$–$4d'$	$[1/2]$–$[1\ 1/2]°$	5912.1	9650–11600	$(1.1$–$5.3) \times 10^{16}$	1.10–6.00				B	[7]
				9100–11450	$(0.63$–$4.70) \times 10^{16}$	0.59–4.62		0.28–2.26		B	[9]
				7800	1.0×10^{16}	0.68		0.38		B	[17]
54.	$4p$–$4d'$	$[2\ 1/2]$–$[1\ 1/2]°$	6538.1	9100–11450	$(0.63$–$4.70) \times 10^{16}$	0.55–4.08		0.29–2.08		B	[9]
55.	$4p$–$4d'$	$[2\ 1/2]$–$[1\ 1/2]°$	6604.0	9100–12700	$(0.63$–$9.4) \times 10^{16}$	0.56–8.40		0.30–2.91		B	[9]
56.	$4p$–$4d'$	$[2\ 1/2]$–$[2\ 1/2]°$	6664.0	9100–10150	$(0.63$–$1.8) \times 10^{16}$	0.52–1.70		0.29–0.74		B	[9]
57.	$4p$–$4d'$	$[1\ 1/2]$–$[2\ 1/1]°$	6879.6	9750–11000	$(1.2$–$3.55) \times 10^{16}$	1.14–3.80		0.51–1.26		B	[9]
58.	$4p$–$6s'$	$[1\ 1/2]$–$[1/2]°$	6698.9	9100–11000	$(0.63$–$3.55) \times 10^{16}$	0.71–3.86		0.49–2.12		B	[9]
59.	$4p$–$4d'$	$[1\ 1/2]$–$[2\ 1/2]°$	6951.5	9750–11000	$(1.2$–$3.55) \times 10^{16}$	1.11–3.04		0.50–1.34		B	[9]
60.	$4p$–$4d'$	$[1\ 1/2]$–$[1\ 1/2]°$	6766.6	9750–11000	$(1.2$–$3.55) \times 10^{16}$	1.71–5.55		0.79–2.06		B	[9]
61.	$4p$–$5s$	$[1/2]$–$[1\ 1/2]°$ (10)	10673.6	10050	1.9×10^{16}	2.4	1.64			C	[6]
62.	$4p$–$5s$	$[2\ 1/2]$–$[1\ 1/2]°$	12487.6	10050	1.9×10^{16}	2.7	1.38			C	[6]
63.	$4p$–$5s$	$[2\ 1/2]$–$[1\ 1/2]°$	12733.6	10050	1.9×10^{16}			0.9		C	[6]
64.	$4p$–$5s$	$[2\ 1/2]$–$[1\ 1/2]°$	12456.1	10050	1.9×10^{16}	2.5				C	[6]
65.	$4p$–$5s$	$[1\ 1/2]$–$[1\ 1/2]°$	13231.4	10050	1.9×10^{16}	4.2				C	[6]
66.	$4p'$–$3d$	$[1\ 1/2]$–$[1\ 1/2]°$	14249.9	10050	1.9×10^{16}	4.1				C	[6]
67.	$4p'$–$5s'$	$[1\ 1/2]$–$[1/2]°$	12933.3	10050	1.9×10^{16}	2.8				C	[6]
68.	$4p'$–$5s'$	$[1\ 1/2]$–$[1/2]°$	13008.5	10050	1.9×10^{16}	3.7	1.70	−0.2	0.19	C	[6]
69.	$4p'$–$5s'$	$[1/2]$–$[1/2]°$	13367.1	10050	1.9×10^{16}			−0.3		C	[6]
70.	$4p$–$5d$	$[1/2]$–$[1/2]°$ (12)	5650.7	9650–11600	$(1.1$–$5.3) \times 10^{16}$	0.9–6.0				B	[7]
				9100–12400	$(0.63$–$7.30) \times 10^{16}$	0.73–9.13		0.23–2.70		B	[9]
				7800	1.0×10^{16}	0.50		0.42		B	[17]
71.	$4p$–$5d$	$[1/2]$–$[1/2]°$	5606.7	9100–12400	$(0.63$–$7.3) \times 10^{16}$	0.77–9.43		0.35–1.80		B	[9]
				7800	1.0×10^{16}	0.72		0.49		B	[17]

No.	Transition array	Transition j-l coupling (Multiplet)	Wavelength (Å)	Temperature (K)	Electron density (cm⁻³)	w_m(Å)	w_m/w_{th}	d_m(Å)	d_m/d_{th}	Acc.	Ref.
72.	$4p$–$5d$	[1/2]–[1 1/2]°	5558.7	9100–12400 7800	$(0.63–7.3) \times 10^{16}$ 1.0×10^{16}	0.87–10.40 0.55	0.69–0.61 0.59	0.48–4.25 0.51	1.00–0.71 0.74	B B	[9] [17]
73.	$4p$–$5d'$	[1/2]–[1 1/2]°	5187.7	9100–11450 7800	$(0.63–4.7) \times 10^{16}$ 1.0×10^{16}	1.26–11.00 1.09		(−0.10)– 0.38 −0.18		B B	[9] [17]
74.	$4p$–$5d$	[2 1/2]–[3 1/2]° (13)	6032.1	9550–11500 9100–11450 7800	$(1.0–5.0) \times 10^{16}$ $(0.63–4.7) \times 10^{16}$ 1.0×10^{16}	1.7–9.2 0.98–8.55 0.75	0.74–0.74 0.69–0.73 0.74	 0.62–3.45 0.81	 1.46–1.05 1.16	B B B	[7] [9] [17]
75.	$4p$–$5d'$	[2 1/2]–[2 1/2]°	5525.0	9100–11000	$(0.63–3.55) \times 10^{16}$	1.28–7.28		0.55–2.03		B	[9]
76.	$4p$–$5d$	[2 1/2]–[3 1/2]°	6043.2	9100–11000 7800	$(0.63–3.55) \times 10^{16}$ 1.0×10^{16}	1.10–6.50 0.90		0.76–2.85 0.99		B B	[9] [17]
77.	$4p$–$5d'$	[2 1/2]–[2 1/2]°	5572.5	9100–11450 7800	$(0.63–4.7) \times 10^{16}$ 1.0×10^{16}	1.27–10.60 1.05	0.95–0.96 1.05	0.53–2.62 0.70	1.12–0.71 0.74	B B	[9] [17]
78.	$4p$–$5d$	[1 1/2]–[1/2]°	6364.9	9100–10150	$(0.63–1.80) \times 10^{16}$	1.12–3.07		0.43–1.60		B	[9]
79.	$4p$–$5d'$	[1 1/2]–[2 1/2]°	5739.5	9550–11500 9100–11450 7800	$(1.0–5.0) \times 10^{16}$ $(0.63–4.7) \times 10^{16}$ 1.0×10^{16}	1.5–9.5 1.22–8.22 0.88	0.70–0.81 0.92–0.75 0.89	 0.54–3.60 0.60	 1.08–1.06 0.88	B B B	[7] [9] [17]
80.	$4p$–$5d$	[1 1/2]–[1/2]°	6369.6	9100–10500	$(0.63–2.47) \times 10^{16}$	1.12–5.28		0.43–1.50		B	[9]
81.	$4p$–$5d$	[1 1/2]–[1 1/2]°	6307.7	9100–11450	$(0.63–4.7) \times 10^{16}$	1.17–9.70		0.72–3.71		B	[9]
82.	$4p$–$5d'$	[1 1/2]–[1 1/2]°	5843.3	9100–10500	$(0.63–2.47) \times 10^{16}$	1.57–6.53		(−0.09)– (−0.13)		B	[9]
83.	$4p$–$5d$	[1/2]–[1/2]°	6719.2	9100–10150	$(0.63–1.80) \times 10^{16}$	1.16–3.96		0.46–1.23		B	[9]
84.	$4p$–$5d'$	[1 1/2]–[2 1/2]°	6105.6	9100–11000	$(0.63–3.55) \times 10^{16}$	1.31–7.80	0.88–0.84	0.61–2.45	1.24–0.86	B	[9]
85.	$4p'$–$5d$	[1 1/2]–[1/2]°	6827.2	9750–10500	$(1.2–2.47) \times 10^{16}$	2.72–4.47		0.87–1.85		B	[9]
86.	$4p'$–$5d'$	[1 1/2]–[2 1/2]°	6145.4	9100–11450	$(0.63–4.7) \times 10^{16}$	1.59–11.90		0.77–4.75		B	[9]
87.	$4p'$–$5d'$	[1/2]–[1 1/2]°	6296.9	9100–11000	$(0.63–3.55) \times 10^{16}$	2.25–11.95	1.64–1.41	(−0.11)–0.0	(−1.42)[a]— 0.54[b]	B	[9]
88.	$4p$–$6s$	[1/2]–[1 1/2]°	6416.3	9100–12400	$(0.63–7.3) \times 10^{16}$	0.53–6.97		0.49–3.69		B	[9]

No.	Transition array	Transition j-l coupling (Multiplet)	Wavelength (Å)	Temperature (K)	Electron density (cm^{-3})	w_{m}(Å)	$w_{\mathrm{m}}/w_{\mathrm{th}}$	d_{m}(Å)	$d_{\mathrm{m}}/d_{\mathrm{th}}$	Acc.	Ref.
89.	4p–6s	[1/2]–[1 1/2]°	6384.7	9100–12400	$(0.63–7.3) \times 10^{16}$	0.56–6.78		0.46–3.60		B	[9]
90.	4p–6s′	[1/2]–[1/2]°	5882.6	9100–11450	$(0.63–4.7) \times 10^{16}$	0.47–3.16		0.20–1.66		B	[9]
91.	4p–6s′	[1/2]–[1/2]°	5860.3	9100–11450	$(0.63–4.7) \times 10^{16}$	0.41–3.64		0.28–2.58		B	[9]
92.	4p–6s′	[2 1/2]–[1/2]°	6431.6	9100–10500	$(0.63–2.47) \times 10^{16}$	0.70–2.90		0.47–1.50		B	[9]
93.	4p–6s′	[1 1/2]–[1/2]°	6660.7	9100–10150	$(0.63–1.8) \times 10^{16}$	0.67–2.19		0.35–0.95		B	[9]
94.	4p–6d	[1/2]–[1/2]°	5151.4	9100–10500 7800	$(0.63–2.47) \times 10^{16}$ 1.0×10^{16}	1.71–6.42 1.18		0.22–1.67		B B	[9] [17]
95.	4p–6d	[1/2]–[1/2]°	5162.3	9100–11450 7800	$(0.63–4.7) \times 10^{16}$ 1.0×10^{16}	1.74–13.00 1.15		0.0–1.05 −0.10		B B	[9] [17]
96.	4p–6d	[2 1/2]–[3 1/2]°	5495.9	9650–11600 9100–12350 7800	$(1.1–5.3) \times 10^{16}$ $(0.63–7.3) \times 10^{16}$ 1.0×10^{16}	2.7–15.0 1.97–25.00 1.68		0.97–8.18 1.18		B B B	[7] [9] [17]
97.	4p–6d	[2 1/2]–[3 1/2]°	5506.1	7800	1.0×10^{16}	1.98		2.01		B	[17]
98.	4p–6d′	[1 1/2]–[2 1/2]°	5254.5	7800	1.0×10^{16}	2.85		0.70		B	[17]
99.	4p′–6d′	[1 1/2]–[2 1/2]°	5559.7	7800	1.0×10^{16}	1.9		0.90		B	[17]
100.	4p–7s	[1/2]–[1 1/2]°	5451.6	9100–11450 7800	$(0.63–4.7) \times 10^{16}$ 1.0×10^{16}	1.04–8.60 0.81		0.80–4.82 0.92		B B	[9] [17]
101.	4p–7s	[2 1/2]–[1 1/2]°	5888.6	9100–12350 7800	$(0.63–7.3) \times 10^{16}$ 1.0×10^{16}	1.18–14.10 0.88	0.70–0.63 0.89	0.90–8.16 0.60	1.13–0.82 0.88	B B	[9] [17]
102.	4p–7s	[2 1/2]–[1 1/2]°	5928.8	9100–11450	$(0.63–4.7) \times 10^{16}$	1.17–8.90		0.85–5.72		B	[9]
103.	4p–7s	[1 1/2]–[1 1/2]°	6098.8	9100–9750	$(0.63–1.2) \times 10^{16}$	1.41–2.62		1.08–2.05		B	[9]
104.	4p–7d	[2 1/2]–[3 1/2]°	5221.3	7800	1.0×10^{16}	3.18		1.9		B	[17]
105.	4p–7d	[2 1/2]–[3 1/2]°	5252.8	7800	1.0×10^{16}	2.8		2.8		B	[17]
106.	4p–8s	[2 1/2]–[1 1/2]°	5421.4	7800	1.0×10^{16}	1.89	0.74	2.36	1.06	B	[17]

ᵃ Shift in direction opposite to theory.
ᵇ Theoretical shift given instead of shift ratio.

7.2. Bromine

Br I

Ground State $1s^22s^22p^63s^23p^63d^{10}4s^24p^5\ ^2P°_{3/2}$

Ionization Potential $11.815\ eV\ =\ 95284.8\ cm^{-1}$

There exists no theoretical comparison for bromine. Since the only results come from the same type of experiment as ref. [1] of Cl I and these lines of Br I are among the strongest in the spectrum, the accuracy is based on comparisons and comments contained in ref. [1] of Cl I.

These results for Br I are given normalized to the electron density of $1.0 \times 10^{17}\ cm^{-3}$.

Reference

[1] Bengtson, R. D., University of Maryland Technical Note BN–559 (1968).

Key data on experiments

Ref.	Plasma source	Method of measurement		Remarks
		Electron density	Temperature	
[1]	Gas-driven shock tube	H_β	Absolute intensity of Ne I 5852 Å line and H_β, also line reversal technique applied to H_α	Photographic technique

Numerical results for Br I

Transition array	Transition (Multiplet)	Wavelength (Å)	Temperature (K)	Electron density (cm⁻³)	w_m(Å)	w_m/w_{th}	d_m(Å)	d_m/d_{th}	Acc.	Ref.
$4p^4(^3P_2)5s–4p^4(^3P_2)6p$	$^4P–^4D°$	4441.7	11000	1.0×10^{17}	10.4				D	[1]
		4525.6	11000	1.0×10^{17}	9.9				D	[1]

7.3. Cadmium

Cd I

Ground State $1s^22s^22p^63s^23p^63d^{10}4s^24p^64d^{10}5s^2\ ^1S_c$

Ionization Potential $8.991\ eV\ =\ 72538.8\ cm^{-1}$

There are no theoretical data to compare with the experimental results, [1], obtained with a pulsed discharge. The results of this experiment are normalized to $N_e = 1.0 \times 10^{17}\ cm^{-3}$ and $T = 11,100$ K. However, large variations of the halfwidths within multiplets seem to indicate that self-absorption has not been corrected properly, especially since the weakest lines have the smallest halfwidth.

Reference

[1] Kusch, H. J. and Oberschelp, E., Z. Astrophys. 67, 85 (1967).

Key data on experiments

Ref.	Plasma source	Method of measurement		Remarks
		Electron density	Temperature	
[1]	Pulsed discharge	H_β	Plasma composition data	Photographic technique

Numerical results for Cd I

Transition array	Transition (Multiplet)	Wavelength (Å)	Temperature (K)	Electron density (cm^{-3})	w_m(Å)	w_m/w_{th}	d_m(Å)	d_m/d_{th}	Acc.	Ref.
$4d^{10}5s5p-4d^{10}5s(^2S)6s$	$^3P°-^3S$ (2)	5085.8	11100	1.0×10^{17}	3.67				D	[1]
		4799.9	11100	1.0×10^{17}	3.84				D	[1]
		4678.2	11100	1.0×10^{17}	1.74				D	[1]
$4d^{10}5s5p-4d^{10}5s(^2S)5d$	$^3P°-^3D$	3610.5	11100	1.0×10^{17}	1.84				D	[1]
		3466.2	11100	1.0×10^{17}	1.63				D	[1]
		3403.6	11100	1.0×10^{17}	0.94				D	[1]

7.4. Calcium

Ca I

Ground State

Ionization Potential

$1s^2 2s^2 2p^6 3s^2 3p^6 4s^2 \; ^1S_0$

6.111 eV = 49304.8 cm^{-1}

Two experimental studies on the broadening of neutral calcium lines have been undertaken with plasmas produced in a pulsed capillary discharge [1] and in a high pressure arc [2].

Only two lines could be compared with theory, and the agreement is very poor. The use of the experimentally determined Stark width of the C I line in [1] (see C I ref. [1]) as an electron density determination makes these results more uncertain. This is mainly due to the experimental results for this C I line differing from theory

by such a large factor and because there was no independent measurement of N_e in either experiment. The results of both experiments have been normalized, ref. [1] to N_e = 1.0 × 10^{18}cm^{-3} and T = 17,600 K and ref. [2] to N_e = 1.0 × 10^{17}cm^{-3} and T = 10,000 K.

References

[1] Kusch, H. J., and Pritschow, H. P., Astron. Astrophys. 4, 31 (1970).

[2] Hühn, R., and Kusch, H. J., Astron. Astrophys. 28, 159 (1973).

Key data on experiments

Ref.	Plasma source	Method of measurement		Remarks
		Electron density	Temperature	
[1]	Pulsed capillary discharge	Stark width of C I line	Relative intensities of Mg II lines	Photographic technique
[2]	High pressure arc	Shift of Ar I line 4158.6 Å composition data, intensity of continuum	Absolute intensity of the Ar I line 4158.6 Å and from relative intensities of Ca I/Ca II lines	Photographic technique

Numerical results for Ca I

Transition array	Transition (Multiplet)	Wavelength (Å)	Temperature (K)	Electron density (cm^{-3})	w_m(Å)	w_m/w_{th}	d_m(Å)	d_m/d_{th}	Acc.	Ref.
$4s3d-3d(^2D)4p$	$^1D-^1F°$ (33)	5349.5	17500	1.0×10^{18}	25.8		3.94		D	[1]
$4s3d-4s(^2S)4f$	$^1D-^1F°$ (35)	4878.1	17500	1.0×10^{18}	44.8		9.30		D	[1]
									D	[2]
$4s4p-4p^2$	$^3P°-^3P$ (5)	4318.6	10000	1.0×10^{17}	0.155					

Numerical results for Ca I—Continued

Transition array	Transition (Multiplet)	Wavelength (Å)	Temperature (K)	Electron density (cm⁻³)	w_m(Å)	w_m/w_{th}	d_m(Å)	d_m/d_{th}	Acc.	Ref
$4s4p$–$4p^2$	$^1P^o$–^1D (47)	5857.4	17500	1.0×10^{18}	46.7		8.17		D	[1
$4s4p$–$4s(^2S)4d$	$^3P^o$–^3D (4)	4425.4	10000	1.0×10^{17}	0.29	0.18			D	[2]
$4s4p$–$4s(^2S)5d$	$^1P^o$–^1D (49)	5188.8	17500	1.0×10^{18}	44.2	0.45	−2.73	0.41	D	[1]

7.5. Carbon

C I

Ground State

$1s^22s^22p^2\ ^3P_0$

Ionization Potential

11.264 eV = 90878.3 cm⁻¹

A variety of plasma sources have been used for investigations of broadening parameters of neutral carbon lines: a pulsed discharge [1], wall-stabilized arcs [2, 4], and a gas-driven shock tube [3]. In all these experiments the plasma was seeded with hydrogen, and H_β was used for the determination of electron density. The measurements were usually performed at a single electron density and temperature, with the exception of an arc experiment [2], where widths of a number of lines were investigated as a function of electron density. It should also be noted that the results reported in ref. [3] are reduced to the specific electron density 1.0×10^{17}cm⁻³.

The results given in the table indicate that self-absorption might not always be properly taken into account. For example, the results for the line 2478.6 Å

differ almost by a factor of eight in two experiments [1, 4]. The curve of growth method was used in ref. [4], and these results are considered more reliable. Also, in ref. [2] differences within multiplet 6 can be noted. The 4762.4 Å line actually consists of two blended lines at the same wavelength but with different j-values. No simple reason, such as optical depth, can be offered to explain the discrepancy within the remaining lines of this multiplet.

References

[1] Kusch, H. J., Z. Astrophys. 67, 64 (1967).
[2] Nubbemeyer, H., and Wende, B., Z. Phys. 225, 69 (1969).
[3] Miller, M. H., and Bengtson, R. D., Phys. Rev. A 1, 983 (1970).
[4] Müller, D., Pichler, G., and Vadla, C., Phys. Lett. 46A, 247 (1973).

Key data on experiments

Ref.	Plasma source	Method of measurement		Remarks
		Electron density	Temperature	
[1]	Pulsed discharge	H_β	Plasma composition data	
[2]	Wall-stabilized arc	H_β	Absolute intensity of Ar II and Ar I lines	
[3]	Gas-driven shock tube	H_β	Absolute line intensities of Ne I 5852.5 Å and H_β	
[4]	Wall-stabilized arc	H_β	Plasma composition data	Curve-of-growth method used to determine Stark width

Numerical results for C I

Transition array	Tran-sition (Multi-plet)	Wave-length (Å)	Temperature (K)	Electron density (cm⁻³)	$w_m(\text{Å})$	w_m/w_{th}	$d_m(\text{Å})$	d_m/d_{th}	Acc.	Ref.
$2p^2-2p(^2P°)3s$	$^1S-^1P°$ (61 uv)	2478.6	12800	1.0×10^{17}	0.54	6.74			D	[1]
			12700	1.0×10^{17}	0.068	0.85			B	[4]
$2p3s-2p(^2P°)4p$	$^3P°-^3S$ (5)	4812.8	10300–11800	$(3.1–7.0) \times 10^{16}$	0.68–1.50	0.84–0.77			C	[2]
		4817.3	10400–11800	$(3.2–7.0) \times 10^{16}$	0.70–1.50	0.84–0.77			C	[2]
		4826.7	10400–11800	$(3.2–7.0) \times 10^{16}$	0.75–1.6	0.93–0.82			C	[2]
$2p3s-2p(^2P°)4p$	$^3P°-^3P$ (6)	4762.4ᵃ	9600–11600	$(1.9–6.4) \times 10^{16}$	0.51–1.82	1.03–0.99			C	[2]
		4766.6	9600–11500	$(1.9–6.1) \times 10^{16}$	0.46–1.22	0.94–0.70			C	[2]
		4771.7	9600–11550	$(1.9–6.2) \times 10^{16}$	0.29–1.06	0.59–0.60			C	[2]
		4775.9	9600–11550	$(1.9–6.2) \times 10^{16}$	0.32–0.99	0.66–0.56			C	[2]
$2p3s-2p(^2P°)4p$	$^1P°-^1P$ (11)	5380.3	9000–11750	$(1.2–7.1) \times 10^{16}$	0.22–1.48	0.78–0.73			C	[2]
			11000	1.0×10^{17}	3.0	1.09	0.3	0.62	C	[3]
$2p3s-2p(^2P°)4p$	$^1P°-^1D$ (12)	5052.1	9000–11750	$(1.2–7.1) \times 10^{16}$	0.51–2.7	1.19–0.97			C	[2]
			11000	1.0×10^{17}	4.0	1.03	2.2	1.21	C	[3]
$2p3s-2p(^2P°)4p$	$^1P°-^1S$ (13)	4932.0	9000–11600	$(1.2–6.4) \times 10^{17}$	0.72–3.17	1.06–0.79			C	[2]
			11000	1.0×10^{17}	4.1	0.66	3.0	0.97	C	[3]

ᵃ Blend.

7.6. Cesium

Cs I

Ground State $1s^2 2s^2 2p^6 3s^2 3p^6 3d^{10} 4s^2 4p^6 5s^2 5p^6 6s \; ^2S_{1/2}$

Ionization Potential $3.893 \text{ eV} = 31406.71 \text{ cm}^{-1}$

Wavelength (Å)	No.	Wavelength (Å)	No.	Wavelength (Å)	No.	Wavelength (Å)	No.
5073.	34	5406.7	7	6010.5	14	6432.0	41
5093.	32	5413.6	25	6034.1	4	6472.6	41
5119.	30	5461.9	10	6116.5	46	6586.5	2
5152.7	28	5465.9	20	6127.5	47	6628.7	40
5196.7	26	5503.9	23	6187.5	45	6723.3	11
5201.	36	5568.4	5	6213.1	16	6824.7	39
5219.	35	5573.7	8	6217.6	15	6870.5	39
5241.	33	5635.2	21	6231.3	44	6973.3	13
5256.6	24	5664.0	17	6250.2	43	6983.5	12
5268.	31	5745.7	6	6288.6	43	7228.5	38
5301.4	9	5838.8	3	6326.2	42	7279.9	38
5303.8	29	5845.1	19	6354.6	1	8015.7	37
5340.9	22	5847.6	18	6365.5	42	8079.0	37
5350.4	27						

The two major contributions out of 11 papers reviewed for the determination of cesium Stark widths [1, 2] are the hollow cathode experiments. Two more line profiles were included from ref. [3], but most other data were not convertible to line widths. The results of [1] and [2] are quite comprehensive and allow some detailed analyses. A very interesting result is the appearance of systematic trends as a function of upper principal quantum numbers. The details are presented in section 4. The results of [1] appear in graphical form again in [4] and [5] so that these results were not analyzed.

The table of data on cesium is arranged according to spectral series, and because there are so many transitions included, a wavelength finding list is also provided. The

measured widths are listed for their respective electron densities and are given for the maximum range in each experiment. The w_m/w_{th} ratio is an average for the experimental conditions, and its scatter over the range of experimental conditions is within the uncertainty presented in the accuracy column. The temperature variations in the experiments were not sufficiently large to demonstrate any temperature dependence of w_m/w_{th} outside the experimental uncertainty.

The multiplicity is given at the beginning of each series, but is not repeated through the entire series. In the fundamental series, no distinction is made in [1] for the different J values in each doublet, and, therefore, a single w_m/w_{th} is given. This can be done because the theoretical widths for different J values for each term in the fundamental series are almost equal.

References

[1] Agnew, L., and Summers, C., Advan. Energy Convers. 3, 7 (1963).
[2] Gridneva, S. M., and Kasabov, G. A., Proc. VIIth Intl. Conl Phen. Ion. Gases, Vol. II, p. 581, Gradevinska Knjiga Pub. House, Belgrade, (1966).
[3] Sayer, B. Sassi, M., and Jeannet, J. C., C. R. H. Acad. Sci. Ser. B 271, 839 (1970).
[4] Agnew, L., and Summers, C., Proc. VIIth Intl. Conf. Phen Ion. Gases, Vol. II, p. 574, Gradevinska Knjiga Publ. House Belgrade, (1966).
[5] Stone, P. M. and Agnew, L., Phys. Rev. 127, 1157 (1962).
[6] Griem, H. R., Plasma Spectroscopy, McGraw-Hill Book Co. Inc., New York, (1964).

Key data on experiments

Ref.	Plasma source	Method of measurement		Remarks
		Electron density	Temperature	
[1]	Hot-cathode parallel geometry cesium diode	Absolute intensity of radiative recombination continuum	Relative intensities of Cs I lines	
[2]	Positive column of low pressure argon-cesium discharge	Absolute intensity of radiative recombination continuum	Relative intensity of recombination continuum	Photographic technique
[3]	Low pressure DC discharge	Microwave interferometer	Not specifically stated	Temperature stated but no measurement details

Numerical results for Cs I

No.	Transition array	Transition (series)	Wavelength (Å)	Temperature (K)	Electron density (cm^{-3})	w_m(Å)	w_m/w_{th}	d_m(Å)	d_m/d_{th}	Acc.	Ref.
		(sharp)									
1.	$6p$–$9s$	$^2P^\circ_{1/2}$–$^2S_{1/2}$	6354.6	6000	1.6×10^{15}	0.5	1.19			D	[1]
2.		$P^\circ_{3/2}$–$S_{1/2}$	6586.5	6000	1.6×10^{15}	0.6	1.34			D	[1]
3.	$6p$–$10s$	$P^\circ_{1/2}$–$S_{1/2}$	5838.8	6000	1.6×10^{15}	1.0	1.21			C	[1]
4.		$P^\circ_{3/2}$–$S_{1/2}$	6034.1	6000	1.6×10^{15}	1.1	1.24			C	[1]
5.	$6p$–$11s$	$P^\circ_{1/2}$–$S_{1/2}$	5568.4	6000	1.6×10^{15}	1.8	1.14			C	[1]
				2380	9.0×10^{13}			0.06	1.50	D	[2]
6.		$P^\circ_{3/2}$–$S_{1/2}$	5745.7	6000	1.6×10^{15}	1.7	0.98			C	[1]
				2380	9.0×10^{13}			0.06	1.50	D	[2]
7.	$6p$–$12s$	$P^\circ_{1/2}$–$S_{1/2}$	5406.7	2380	9.0×10^{13}			0.10	1.41	D	[2]
8.		$P^\circ_{3/2}$–$S_{1/2}$	5573.7	2380	9.0×10^{13}			0.12	1.60	D	[2]

Numerical results for Cs I—Continued

No.	Tran-sition array	Transition (series)	Wave-length (Å)	Temper-ature (K)	Electron density (cm⁻³)	w_m(Å)	w_m/w_{th}	d_m(Å)	d_m/d_{th}	Acc.	Ref.
9.	6p–13s	P°₁/₂–S₁/₂	5301.4	2380	9.0×10^{13}			0.16	1.23	D	[2]
10.		P°₃/₂–S₁/₂	5461.9	2380	9.0×10^{13}			0.16	1.33	D	[2]
		(diffuse)									
11.	6p–7d	²P°₁/₂–²D₃/₂	6723.3	6000	1.6×10^{15}	0.5	1.18			D	[1]
12.		P°₃/₂–D₃/₂	6983.5	6000	1.6×10^{15}	0.6	1.32ᵃ			D	[1]
13.		P°₃/₂–D₅/₂	6973.3	6000	1.6×10^{15}	0.8	1.58			C	[1]
14.	6p–8d	P°₁/₂–D₃/₂	6010.5	6000	$(1.3–1.6) \times 10^{15}$	0.9–1.3	1.50			C	[1]
15.		P°₃/₂–D₃/₂	6217.6	2360–6000	$(0.28–1.6) \times 10^{15}$	0.4–1.3	1.26ᵃ			C	[1]
16.		P°₃/₂–D₅/₂	6213.1	2360–6000	$(0.28–1.6) \times 10^{15}$	0.4–1.5	1.58			C	[1]
17.	6p–9d	P°₁/₂–D₃/₂	5664.0	6000	$(1.3–1.6) \times 10^{15}$	2.0–2.1	1.12			C	[1]
18.		P°₃/₂–D₃/₂	5847.6	2400	0.39×10^{15}	0.5	1.01ᵃ			D	[1]
19.		P°₃/₂–D₅/₂	5845.1	2400–6000	$(0.39–1.6) \times 10^{15}$	0.6–2.8	1.18			C	[1]
20.	6p–10d	P°₁/₂–D₃/₂	5465.9	6000 2380	1.3×10^{15} 9.0×10^{13}	3.2 0.28	1.02 1.60	−0.04	1.50	C D	[1] [2]
21.		P°₃/₂–D₅/₂	5635.2	6000 2380	1.3×10^{15} 9.0×10^{13}	3.9 0.35	1.01 1.59	−0.05	1.11	C D	[1] [2]
22.	6p–11d	P°₁/₂–D₃/₂	5340.9	6000 2380	1.3×10^{15} 9.0×10^{13}	5.3 0.35	0.94 1.09	−0.06	1.03	C D	[1] [2]
23.		P°₃/₂–D₅/₂	5503.9	6000 2380	1.3×10^{15} 9.0×10^{13}	5.1 0.44	0.74 1.00	−0.05	0.71	C D	[1] [2]
24.	6p–12d	P°₁/₂–D₃/₂	5256.6	2380	9.0×10^{13}	0.60	1.07	−0.09	1.12	D	[2]
25.		P°₃/₂–D₅/₂	5413.6	2380	9.0×10^{13}	0.70	1.03	−0.10	1.00	D	[2]
26.	6p–13d	P°₁/₂–D₃/₂	5196.7	2380	9.0×10^{13}	0.84	0.93	−0.11	0.92	D	[2]
27.		P°₃/₂–D₅/₂	5350.4	2380	9.0×10^{13}	1.04	0.94	−0.15	1.00	D	[2]
28.	6p–14d	P°₁/₂–D₃/₂	5152.7	2380	9.0×10^{13}	1.2	0.85	−0.21	1.05	D	[2]
29.		P°₃/₂–D₅/₂	5303.8	2380	9.0×10^{13}	1.5	0.87	−0.22	1.05	D	[2]
30.	6p–15d	P°₁/₂–D₃/₂	5149.0	2380	9.0×10^{13}	2.0	0.95	−0.20	0.83	D	[2]
31.		P°₃/₂–D₅/₂	5268.0	2380	9.0×10^{13}	2.3	0.85	−0.24	0.77	D	[2]
32.	6p–16d	P°₁/₂–D₃/₂	5093.0	2380	9.0×10^{13}	3.5	1.09			D	[2]
33.		P°₃/₂–D₅/₂	5241.0	2380	9.0×10^{13}	3.7	0.92			D	[2]
34.	6p–17d	P°₁/₂–D₃/₂	5073.0	2380	9.0×10^{13}	4.3	0.98			D	[2]
35.		P°₃/₂–D₅/₂	5219.0	2380	9.0×10^{13}	5.3	0.91			D	[2]
36.	6p–18d	P°₃/₂–D₅/₂	5201.0	2380	9.0×10^{13}	7.8	0.95			D	[2]

Numerical results for Cs I—Continued

No.	Transition array	Transition (series)	Wavelength (Å)	Temperature (K)	Electron density (cm⁻³)	w_m(Å)	w_m/w_{th}	d_m(Å)	d_m/d_{th}	Acc.	Ref.
		(fundamental)									
37.	$5d$–$5f$	^2D–$^2F°$	8015.7 8079.0	2400–6000	$(0.39$–$1.6) \times 10^{15}$	0.6–2.3	1.34			C	[1]
38.	$5d$–$6f$	D–F°	7228.5 7279.9	2400–6000	$(0.39$–$1.6) \times 10^{15}$	1.1–5.4	1.07			C	[1]
39.	$5d$–$7f$	D–F°	6824.7 6870.5	2360–6000	$(0.28$–$1.6) \times 10^{15}$	1.7–12.2	1.09			C	[1]
40.	$5d$–$8f$	D–F°	6628.7	2500–6000	$(0.11$–$1.6) \times 10^{15}$	1.6–20.5	0.99			C	[1]
41.	$5d$–$9f$	D–F°	6432.0 6472.6	2500–2670	$(1.1$–$3.3) \times 10^{14}$	2.6–6.3	1.05			C	[1]
		$D_{3/2}$–$F°_{5/2}$	6432.0	2380	9.0×10^{13}	1.75	0.88	0.4	1.00	D	[2]
		$D_{5/2}$–$F°_{7/2}$	6472.6	2380	9.0×10^{13}	1.8	0.90	0.4	1.00	D	[2]
42.	$5d$–$10f$	D–F°	6326.2 6365.5	2500–2670	$(1.1$–$3.3) \times 10^{14}$	4.2–10.0[b]	1.19			D	[1]
		$D_{3/2}$–$F°_{5/2}$	6326.2	2380	9.0×10^{13}	2.9	0.91	0.5	0.83	D	[2]
		$D_{5/2}$–$F°_{3/2}$	6365.5	2380	9.0×10^{13}	2.9	0.91	0.5	0.83	D	[2]
43.	$5d$–$11f$	D–F°	6250.2 6288.6	2200–2570	$(0.44$–$1.4) \times 10^{14}$	1.8–7.8				C	[1]
		$D_{3/2}$–$F°_{5/2}$	6250.2	2380	9.0×10^{13}	3.75		0.7		D	[2]
		$D_{5/2}$–$F°_{7/2}$	6288.6	2380	9.0×10^{13}	3.9		0.7		D	[2]
44.	$5d$–$12f$	$D_{5/2}$–$F°_{7/2}$	6231.3	2150–2200 2380	$(3.2$–$4.4) \times 10^{13}$ 9.0×10^{13}	1.4–2.4 5.45				C D	[1] [2]
45.	$5d$–$13f$	$D_{5/2}$–$F°_{7/2}$ $D_{5/2}$–$F°_{5/2, 7/2}$	6187.5	2380 2000	9.0×10^{13} 2.1×10^{13}	7.2 1.75				D D	[2] [3]
46.	$5d$–$14f$	$D_{3/2}$–$F°_{5/2}$	6116.5	2380	9.0×10^{13}	9.6				D	[2]
47.	$5d$–$15f$	$D_{5/2}$–$F°_{5/2, 7/2}$	6127.5[c]	2000	2.1×10^{13}	1.15				D	[3]

[a] Obtained using [6], page 454.
[b] Possible blending of $5d$–$10g$ forbidden transition [5].
[c] Calculated wavelength.

7.7. Chlorine

Cl I

Ground State	$1s^2 2s^2 2p^6 3s^2 3p^5\ {}^2P^\circ_{3/2}$
Ionization Potential	13.01 eV = 104991 cm^{-1}

Both sets of experimental data were obtained in transient plasma sources: a gas-driven shock tube [1] and a low-pressure pulsed arc [2]. In both cases results are given normalized to the electron density of 1.0×10^{17} cm^{-3}.

The results of ref. [2] are in good agreement compared with theory. On the other hand, widths and shifts of ref. [1] are systematically larger. Also, large variations for ref. [1] w_m/w_{th} ratios for different lines of multiplet

2 were noted as a function of line intensity. This is usually an indication that self-absorption is not taken into account properly, and, therefore, preference should be given to the data reported in ref. [2].

References

[1] Miller, M. H., and Bengtson, R. D., Phys. Rev. A 1 983 (1970).
[2] Konjevic, N., Platisa, M., and Labat, J., Phys. Lett. 32A 420 (1970); Puric, J., Konjevic, N., Platisa, M., and Labat, J., Phys. Lett. 37A, 425 (1971).

Key data on experiments

Ref.	Plasma source	Method of measurement		Remarks
		Electron density	Temperature	
[1]	Gas-driven shock tube	H$_\beta$	Absolute intensity of Ne I 5852 Å line and H$_\beta$, also line reversal technique applied to H$_\alpha$	Photographic technique
[2]	Low-pressure pulsed arc	Laser interferometry	Relative intensities of Cl I/Cl II line	

Numberical results for Cl I

Transition array	Transition (Multiplet)	Wavelength (Å)	Temperature (K)	Electron density (cm^{-3})	w_m(Å)	w_m/w_{th}	d_m(Å)	d_m/d_{th}	Acc.	Ref.
$3p^4 4s-3p^4(^3P)4p$	$^4P-^4D^\circ$ (2)	8428.2	11000	1.0×10^{17}	3.3	2.20			D	[1]
			9500	1.0×10^{17}	1.61	1.10			C	[2]
		8212.0	11000	1.0×10^{17}	3.5	2.33			D	[1]
			9500	1.0×10^{17}	1.56	1.07			C	[2]
		8194.4	11000	1.0×10^{17}	2.1	1.40			D	[1]
			9500	1.0×10^{17}	1.70	1.16			C	[2]
$3p^4 4s-3p^4(^3P)4p$	$^4P-^2D^\circ$ (3)	7878.2	11000	1.0×10^{17}	4.2				D	[1]
$3p^4 4s-3p^4(^3P)4p$	$^4P-^2P^\circ$ (4)	7717.6	11000	1.0×10^{17}	1.7				D	[1]
		7414.1	11000	1.0×10^{17}	1.7				D	[1]
		7924.6	9500	1.0×10^{17}	1.32		0.65		C	[2]
$3p^4 4s-3p^4(^3P)4p$	$^4P-^4S^\circ$ (5)	7744.9	11000	1.0×10^{17}	2.8	1.39			D	[1]
			9500	1.0×10^{17}	1.47	0.86	0.7	0.88	C	[2]
		7256.6	11000	1.0×10^{17}	2.8	1.39	1.1	1.37	D	[1]
$3p^4 4s-3p^4(^3P)4p$	$^2P-^4S^\circ$ (14)	8686.3	11000	1.0×10^{17}	1.6				D	[1]
			9500	1.0×10^{17}	1.10				C	[2]
$3p^4 4s-3p^4(^3P)5p$	$^4P-^4P^\circ$ (6)	4438.5	11000	1.0×10^{17}	7.3				D	[1]
$3p^4 4s-3p^4(^3P)5p$	$^2P-^2P^\circ$ (15)	4601.0	11000	1.0×10^{17}	5.8	1.20			C	[1]
		4526.2	11000	1.0×10^{17}	5.7	1.18			C	[1]

7.8. Fluorine

F I

Ground State $1s^2 2s^2 2p^5\ {}^2P^\circ_{3/2}$

Ionization Potential $17.42\ eV = 140553.5\ cm^{-1}$

There is only one paper which reports Stark broadening data of neutral fluorine lines. These have been measured in a low pressure pulsed arc [1], where a laser interferometer was used to determine the electron concentration. The agreement with the theory is generally poor. For example, some line shift measurements (multiplet no. 1) gave values five times larger than theoretical, while the widths of lines belonging to multiplet nos. 5 and 6 are four times smaller than theoretically predicted. While this experiment was performed in a relatively high electron density—temperature range and the theory gave larger widths than were measured in a number of cases at higher temperatures—it was not possible to find a simple explanation for the large discrepancies with the theory. As a result, additional experiments are very desirable.

Reference

[1] Konjevic, N., Platisa, M., and Popovic, M., Z. Phys. 257, 235 (1972).

Key data on experiments

Ref.	Plasma source	Method of measurement		Remarks
		Electron density	Temperature	
[1]	Pulsed low pressure arc	Laser interferometry	Relative intensity of Cl II lines	Instrument function half-width comparable to measured Stark widths

Numerical results for F I

Transition array	Transition (Multiplet)	Wavelength (Å)	Temperature (K)	Electron density (cm^{-3})	w_m(Å)	w_m/w_{th}	d_m(Å)	d_m/d_{th}	Acc.	Ref.
$2p^43s-$	$^4P-^4P^\circ$	7331.9	19100–36200	$(0.71-1.43) \times 10^{17}$	0.21–0.46	0.55–0.32	0.08–0.14	4.80–5.50	C	[1]
$2p^4(^3P)3p$	(1)	7398.7	19100–28200	$(0.71-1.21) \times 10^{17}$	0.23–0.39	0.60–0.36	0.08–0.12	4.80–5.46	C	[1]
$2p^43s-$	$^4P-^4D^\circ$	6902.5	19100–36200	$(0.71-1.43) \times 10^{17}$	0.24–0.49	0.52–0.40	0.09–0.16	0.81–0.78	C	[1]
$2p^4(^3P)3p$	(2)	6856.0	19100–36200	$(0.71-1.43) \times 10^{17}$	0.24–0.49	0.52–0.40	0.11–0.17	0.88–0.83	C	[1]
$2p^43s-$	$^4P-^4S^\circ$	6239.6	19100–29400	$(0.71-1.15) \times 10^{17}$	0.23–0.39	0.49–0.43	0.10–0.15	0.54–0.51	C	[1]
$2p^4(^3P)3p$	(3)	6413.7	23650–36200	$(0.91-1.43) \times 10^{17}$	0.29–0.49	0.45–0.40	0.13–0.19	0.56–0.54	C	[1]
		6348.5	19100–36200	$(0.71-1.43) \times 10^{17}$	0.23–0.49	0.49–0.40			C	[1]
$2p^43s-$	$^2P-^2S^\circ$	7311.0	23650–36200	$(0.91-1.43) \times 10^{17}$	0.22–0.37	0.25–0.22	(−0.11)–(−0.13)	(−0.52)–(−0.42)^a	C	[1]
$2p^4(^3P)3p$	(5)									
$2p^43s-$	$^2P-^2P^\circ$	7037.5	23650–28200	$(0.91-1.21) \times 10^{17}$	0.20–0.29	0.25–0.23	(−0.13)–(−0.16)	(−0.48)–(−0.45)^a	C	[1]
$2p^4(^3P)3p$	(6)	7127.9	28200	1.21×10^{17}	0.29	0.24	−0.15	−0.43^a	C	[1]

^{a} Theory predicts shift in opposite direction.

7.9. Germanium

Ge I

Ground State	$1s^22s^22p^63s^23p^63d^{10}4s^22p^2$ $^3P_0$
Ionization Potential	7.91 eV = 63715 cm^{-1}

Only one paper deals with the Stark broadening of germanium [1], and there is no direct comparison with ref. [1] of the general references. The w_m values are normalized to $N_e = 1.0 \times 10^{17}$ cm^{-3} and $T = 11,000$ K.

Reference

[1] Jones, W. W., and Miller, M. H., Phys. Rev. A **10**, 1803 (1974).

Key data on experiments

Ref.	Plasma source	Method of measurement		Remarks
		Electron density	Temperature	
[1]	Gas-driven shock tube	H$_\beta$	Line reversal technique applied to H$_\alpha$, absolute intensities of H$_\beta$ and 5853 Å Ne I lines	Photographic technique, carbon arc calibration

Numerical results for Ge I

Transition array	Transition (Multiplet)	Wavelength (Å)	Temperature (K)	Electron density (cm^{-3})	w_m(Å)	w_m/w_{th}	d_m(Å)	d_m/d_{th}	Acc.	Ref.
4p–5s	^{1}D–^{3}P°	4684.8	11000	1.0×10^{17}	0.35				C	[1]
	^{1}S–^{1}P°	4226.2	11000	1.0×10^{17}	3.18				C	[1]

7.10. Helium

He I

Ground State	$1s^2$ $^1S_0$
Ionization Potential	24.580 eV = 198305 cm^{-1}

Of the ten refs. [1–10] selected, all but two [6, 7] used transient sources to observe helium Stark widths. Only papers dealing with optically allowed (LS coupling) helium transitions unblended with other allowed or forbidden transitions were used. In refs. [5] and [6] best fit values over the range to electron density were used, and in ref. [6] only the results where instrument and Doppler broadening were not appreciable were used. This is because for comparison purposes in ref. [6] these two broadening mechanisms were convoluted into the theory rather than deconvoluted from the experimental results. The results of ref. [4] do not represent a range of

values but results for the specific electron densities and temperatures stated. The shift results of ref. [7] were originally given as a wavelength shift of the median rather than the wavelength shift of the peak intensity. This is due to the fact that the helium lines observed in this experiment had slight asymmetries. These results presented here were converted to wavelength shifts of the peak intensity. The results of ref. [4] are the renormalized results of ref. [10]. The results of ref. [10] are not included because of the line profile normalization procedure for different electron densities. The condition of ref. [9] results in a value of R (see section 3) slightly

larger than 0.8; however, eq (15) was used to determine the theoretical width for comparison.

References

[1] Lincke, R., Thesis, University of Maryland (1964).

[2] Berg, H. F., Ali, A. W., Lincke, R., and Griem, H. R., Phys. Rev. 125, 199 (1962).

[3] Wulff, H., Z. Phys. 150, 614 (1958).

[4] Greig, J. R., and Jones, L. A., Phys. Rev. A 1, 1261 (1970).

[5] Kusch, H. J., Z. Naturforsch. A 26, 1970 (1971).

[6] Bötticher, W., Roder, O., and Wobig, K. H., Z. Phys. 175, 480 (1963).

[7] Morris, R. N., and Cooper, J., Can. J. Phys. 51, 1746 (1973).

[8] Jenkins, J. E., and Burgess, D. D., J. Phys. B 4, 1353 (1971).

[9] Puric, J., Labat, J., Cirkovic, Lj., and Konjevic, N., Fizika 2, 67 (1970).

[10] Greig, J. R., Lim, C. P., Moo-Young, G. A., Palumbo, G., and Griem, H. R., Phys. Rev. 172, 148 (1968).

[11] Roder, O., and Stampa, A., Z. Phys. 178, 348 (1964).

Key data on experiments

Ref.	Plasma source	Method of measurement		Remarks
		Electron density	Temperature	
[1]	Electric T-tube	H_α, H_β, H_γ, 3889 Å He I line profiles and absolute hydrogen plus helium continuum intensity	Hydrogen line-to-continuum intensity ratio	Carbon arc calibration
[2]	Electric T-tube	Absolute hydrogen plus helium continuum intensity	He II/He I line intensity ratio	Carbon arc calibration
[3]	Low pressure pulsed arc	Inglis-Teller limit and composition data	He II/He I line intensity ratio	
[4]	Electric T-tube	H_β	Ratio H_β/continuum intensities	
[5]	Pulsed arc	H_β	Ratio H_β/continuum intensities	Photographic technique
[6]	Wall-stabilized arc	Absolute intensities of He I lines	Absolute intensities of He I lines	Photographic technique and carbon arc calibration
[7]	Plasma jet	Stark widths of H_β and He I 5016 Å and 4921 Å lines	Absolute intensities of He I lines	
[8]	Z-pinch discharge	Laser interferometry	He II/He I line intensity ratio	
[9]	Electric shock tube	H_β	Relative intensities of He I lines	

Numerical results for He I

Transition array	Transition (Multiplet)	Wavelength (Å)	Temperature (K)	Electron density (cm^{-3})	w_m(Å)	w_m/w_{th}	d_m(Å)	d_m/d_{th}	Acc.	Ref.
1s2s–1s3p	$^1S-^1P°$ (4)	5015.7	22700	9.3×10^{16}	7.2	0.86	−1.7	0.66	B	[1]
			24000	1.65×10^{17}	13.0	0.86	−4.8	0.98	B	[2]
			30000	3.2×10^{16}	1.9	0.72			B	[3]
			25000&23000	$(0.27\&1.7) \times 10^{17}$	2.77&18.4	1.20&1.17			C	[4]
			18000–26000	$(0.8–4.6) \times 10^{16}$	0.11–0.75	1.66–1.86			D	[5]
			15600–16900	$(1.0–2.0) \times 10^{16}$	0.95–1.6	1.13–0.94	(−0.18)–(−0.43)	0.69–0.80	C	[6]
			10000–16000	$(0.6–2.3) \times 10^{16}$			(−0.24)–(−0.55)	1.26–0.87	B	[7]

Numerical results for He I—Continued

Transition array	Transition (Multiplet)	Wavelength (Å)	Temperature (K)	Electron density (cm⁻³)	w_m(Å)	w_m/w_{th}	d_m(Å)	d_m/d_{th}	Acc.	Ref.
1s2p-1s4s	¹P°-¹S (47)	5047.7	30000	3.2 × 10¹⁶	4.6	0.78			B	[3]
			14500-16900	(0.5-2.0) × 10¹⁶	1.2-3.4	0.98-0.60	0.35-1.4	0.58-0.50	C	[6]
1s2p-1s5s	¹P°-¹S (50)	4437.6	14500-15600	(0.5-1.0) × 10¹⁶	2.25-4.25	1.14-1.05	1.0-2.0	1.14-1.10	C	[6]
1s2p-1s5d	¹P°-¹S (51)	4387.9	14500-15100	(0.5-0.75) × 10¹⁶	6.0-10.0	0.49-0.52	0.3-0.5	0.059-0.061	C	[6]
1s2s-1s3p	³S-³P° (2)	3888.7	26000	1.5 × 10¹⁷	4.5	1.11	1.2	1.27	B	[2]
			30000	3.2 × 10¹⁶	0.73	0.87			B	[3]
			18000-26000	(0.8-4.6) × 10¹⁶	0.33-2.31	1.64-1.88			D	[5]
			14500-18000	(0.5-3.5) × 10¹⁶			0.06-0.22	1.91-0.99	C	[6]
			10000-16000	(0.6-2.3) × 10¹⁶			0.06-0.19	1.44-1.25	B	[7]
1s2s-1s4p	³S-³P° (3)	3187.7	29000	1.5 × 10¹⁷	13.4	1.00	4.1	1.19	B	[2]
1s2s-1s5p	³S-³P° (11 uv)	2945.1	40000	1.2 × 10¹⁶	2.5	0.98			C	[8]
1s2p-1s4s	³P°-³S (12)	4713.2	22700	9.3 × 10¹⁶	9.1	0.91	4.3	0.96	B	[1]
			20000	1.3 × 10¹⁷	14.0	1.02	6.0	0.93	B	[2]
			30000	3.2 × 10¹⁷	2.9	0.85			B	[3]
			10000-16000	(0.6-2.3) × 10¹⁶	0.52-1.29		0.52-1.29	1.44-1.19	B	[7]
1s2p-1s5s	³P°-³S (16)	4120.8	30000	3.2 × 10¹⁶	6.2	0.77			B	[3]
			14500-16900	(0.5-2.0) × 10¹⁶	1.6-4.2	0.85-0.48	0.65-1.85	1.08-0.59	C	[6]
1s2p-1s3d	³P°-³D (11)	5875.7	43000&45000	(1.26&1.59) × 10¹⁷	4.9&5.5	0.96&0.89	0.0&0.7	(−0.82)ᵃ-(−0.78)	B	[2]
			3700-4900	(2.25-3.45) × 10¹⁶	0.91-1.35	1.25-1.15			C	[9]

ᵃ Theoretical shift.

7.11. Lithium

Li I

Ground State

Ionization Potential

$1s^22s\ ^2S_{1/2}$

$5.390\ eV = 43487.19\ cm^{-1}$

For Li I a total of 12 papers were reviewed. Of these only 3 papers [1-3] provide sufficient information according to our criteria to ascertain that reliable data have been produced. One of these, [3], reports the width of a single transition (4132.6 Å) as a function of N_e. The ratio of the measured to theoretical widths demonstrated a systematic variation of a factor of two over the range of N_e from 3.0-8.0 × 10¹⁴ cm⁻³ implying problems in the source and, therefore, was not included in the final results. A total of four transitions were analyzed. The w_m/w_{th} ratios are taken from a fitted value as presented in [1] for $N_e = 2.0 × 10^{17}$ cm⁻³ and a constant temperature ($T = 11,000$ K). This could be done since the random variation over the narrow experimental temperature range is well within the uncertainty. Since the 3232.6 Å line is a resonance transition, optical thickness may be a problem as indicated by $w_m/w_{th} = 2.04$, and, therefore, this result is less reliable. It should also be noted that for the 2p-4d and 5d transitions the theoretical A values (see section 3) are greater than 0.5; however, eq (15) was used to determine the theoretical width for comparison.

References

[1] Heyde, R. von der, and Kusch, H. J., Z. Astrophys. 68, 1 (1968).
[2] Ya'akobi, B., Phys. Rev. 176, 227 (1968).
[3] Zhirnov, V. A., and Tetyukhin, Yu. A., Zh. Prikl. Spektrosk. 18, 596 (1973).

Key data on experiments

Ref.	Plasma source	Method of measurement		Remarks
		Electron density	Temperature	
[1]	Pulsed capillary discharge	H_β	Plasma composition data	Photographic technique
[2]	Exploding lithium wire	Inglis-Teller formula, Saha equation	Electrical conductivity, recombination continuum	Photographic technique

Numerical results for Li I

Transition array	Transition (Multiplet)	Wavelength (Å)	Temperature (K)	Electron density (cm^{-3})	$w_m(Å)$	w_m/w_{th}	$d_m(Å)$	d_m/d_{th}	Acc.	Ref.
$2s-3p$	$^2S-^2P^\circ$ (2)	3232.6	10500-11500	$(0.8-3.2) \times 10^{17}$	3.3-13.4	2.04[a]	0.75-3.1	1.31[a]	D	[1]
$2p-4s$	$^2P^\circ-^2S$ (5)	4971.7	10500-11500	$(0.8-3.2) \times 10^{17}$	4.8-20.0	0.89[a]			C	[1]
$2p-4d$	$^2P^\circ-^2D$ (6)	4602.9	10500-11500	$(0.8-3.2) \times 10^{17}$	42.0-172.0	0.71[a]			C	[1]
$2p-5d$	$^2P^\circ-^2D$	4132.6	10500-11500	$(0.8-3.2) \times 10^{17}$	29.0-114.0	0.12[a]			C	[1]
			10000	2.5×10^{17}	94.2	0.13			C	[2]

[a] Values taken at 2.0×10^{17} cm^{-3}.

7.12. Magnesium

Mg I

Ground State $1s^2 2s^2 2p^6 3s^2$ $^1S_0$

Ionization Potential   7.644 eV = 61699.14 cm^{-1}

There is very little data on the broadening of neutral magnesium lines. Only one paper reports Stark widths and shifts for two lines, 5528.4 Å and 4703.0 Å. The plasma source was a high pressure argon arc (up to 150 atm) with magnesium evaporating from the anode. At this pressure, van der Waals broadening was always comparable with Stark broadening, and this was taken into account. The results of this experiment are normal-ized to $N_e = 1.0 \times 10^{17}$ and $T = 10,000$ K. The experimental Stark shifts and widths are much smaller than theoretical predictions. No ready explanation for this discrepancy was found, and new experiments at lower pressures would be most desirable.

Reference

[1] Helbig, V. and Kusch, H. J., Astron. Astrophys. 20, 299 (1972)

Key data on experiments

Ref.	Plasma source	Method of measurement		Remarks
		Electron density	Temperature	
[1]	Gas stabilized high pressure arc	Shift of Ar I 4158 Å line, absolute intensity of Mg I and Mg II lines, and from Ar I continuum at 3600 Å	Absolute intensity of Ar I 3158.6 Å line and Mg I/Mg II relative intensities	Photographic technique, van der Waals broadening comparable to Stark broadening

Numerical results for Mg I

Transition array	Transition (Multiplet)	Wavelength (Å)	Temperature (K)	Electron density (cm⁻³)	w_m(Å)	w_m/w_{th}	d_m(Å)	d_m/d_{th}	Acc.	Ref.
$3s3p-3s(^2S)4d$	$^1P°-^1D$ (9)	5528.4	10000	1.0×10^{17}	2.14	0.40	1.88	0.69	D	[1]
$3s3p-3s(^2S)5d$	$^1P°-^1D$ (11)	4703.0	10000	1.0×10^{17}	4.22	0.35	1.98	0.36	D	[1]
$3s(^2S)3d-3p(^2P°)3d$	$^1D-^1F°$ (15)	2915.5	10000	1.0×10^{17}	0.25		−0.06		D	[1]

7.13. Neon

Ne I

Ground State $\qquad\qquad\qquad\qquad\qquad\qquad\qquad\qquad\qquad\qquad$ $1s^2 2s^2 2p^6\ {}^1S_0$

Ionization Potential $\qquad\qquad\qquad\qquad\qquad\qquad$ 21.559 eV = 173931.7 cm⁻¹

Wavelength (Å)	Number	Wavelength (Å)	Number	Wavelength (Å)	Number	Wavelength (Å)	Number
735.9	2	5881.9	7	6266.5	13	6532.9	12
743.7	1	5944.8	6	6334.4	4	6599.0	18
5441.1	20	6074.4	10	6383.0	9	6678.3	17
5764.4	21	6096.2	11	6402.2	3	6717.0	16
5820.2	22	6143.1	5	6506.5	8	6929.0	15
5852.5	19	6163.6	14				

Four papers report broadening parameters of neon lines [1–4], with most of the data provided by measurements with a wall-stabilized arc for a number of electron densities and temperatures [2]. Vacuum ultraviolet lines were measured in an electric T-tube [1], while the visible lines were measured in a gas-driven shock tube and electric T-tube [3]. All these experiments were seeded with hydrogen, and H_β was used for the determination of electron density. The results of ref. [3] were normalized to an electron density of 1.0×10^{17} cm⁻³.

It is interesting to note that according to the data table theory almost always predicted larger widths than were experimentally measured, with the exception of the 5852.5 Å line. Since the 5852.5 Å line of multiplet 6 is the strongest line of the multiplet, optical thickness may be a problem (as is indicated by its larger w_m/w_{th} ratio), especially at lower electron densities and thus narrower widths.

References

[1] Moo-Young, G. A., Greig, J. R., and Griem, H. R., Phys. Rev. A 2, 1617 (1970).

[2] Nubbemeyer, H., Stuck, D., and Wende, B., Z. Phys. 234, 29 (1970).

[3] Miller, M. H., and Bengtson, R. D., Phys. Rev. A 1, 983 (1970).

[4] Miller, M. H., Roig, R. A., and Moo-Young, G. A., Phys. Rev. A 4, 971 (1971).

Key data on experiments

Ref.	Plasma source	Method of measurement		Remarks
		Electron density	Temperature	
[1]	Electric T-tube	H_β	Relative intensity of Ne I 5882 Å/H_β lines	Lorentz fitted optically thick lines
[2]	Wall-stabilized arc	H_β	Absolute intensities of Ar I and Ar II lines, composition data	
[3]	Gas-driven shock tube	H_β	Absolute line intensities of Ne I 5852.5 Å and H_β	Photographic technique
[4]	Gas-driven shock tube	H_β	Absolute line intensities of Ne I 5852.5 Å and H_β	Photographic technique

No.	Transition array	Transition (jl-coupling) (Multiplet)	Wavelength (Å)	Temperature (K)	Electron density (cm⁻³)	w_m(Å)	w_m/w_{th}	d_m(Å)	d_m/d_{th}	Acc.	Ref.
1.	$2p^6$–$2p^5(^2P°_{1\ 1/2})3s$	^1S–[1 1/2]° (1 uv)	743.7	16100	7.8×10^{16}	2.03×10^{-3}	0.62			D	[1]
2.	$2p^6$–$2p^5(^2P°_{1/2})3s'$	^1S–[1/2]° (2 uv)	735.9	16100	7.8×10^{16}	1.87×10^{-3}	0.56			D	[1]
3.	$2p^53s$–$2p^5(^2P°_{1\ 1/2})3p$	[1 1/2]°–[2 1/2] (1)	6402.2	11650–13600	$(0.5–1.25) \times 10^{17}$	0.20–0.49	0.96–0.91			B	[2]
4.		[1 1/2]°–[1 1/2]	6334.4	11650–13600	$(0.5–1.25) \times 10^{17}$	0.15–0.38	0.72–0.71			B	[2]
5.		[1 1/2]°–[1/2]	6143.1	11650–13600	$(0.5–1.25) \times 10^{17}$	0.20–0.41	0.96–0.76			B	[2]
6.	$2p^5(^2P°_{1\ 1/2})3s$–$2p^5(^2P°_{1/2})3p'$	[1 1/2]°–[1 1/2] (1)	5944.8	11650–13600	$(0.5–1.25) \times 10^{17}$	0.17–0.50	0.91–0.77			B	[2]
7.	$2p^5(^2P°_{1/2})3p'$	[1 1/2]°–[1/2]	5881.9	11650–13600	$(0.5–1.25) \times 10^{17}$	0.16–0.38	0.86–0.71			B	[2]
8.	$2p^53s$–$2p^5(^2P°_{1\ 1/2})3p$	[1 1/2]°–[2 1/2] (3)	6506.5	11650	1.0×10^{17}	0.45	1.01	0.23	1.30	C	[4]
9.		[1 1/2]°–[1 1/2]	6383.0	11650–13600	$(0.5–1.25) \times 10^{17}$	0.17–0.42	0.76–0.71			B	[2]
10.		[1 1/2]°–[1/2]	6074.3	11650–13600	$(0.5–1.25) \times 10^{17}$	0.16–0.39	0.72–0.66			B	[2]
11.	$2p^5(^2P°_{1\ 1/2})3s$–$2p^5(^2P°_{1/2})3p'$	[1 1/2]°–[1 1/2] (3)	6096.2	11650–13600	$(0.5–1.25) \times 10^{17}$	0.18–0.43	0.88–0.79			B	[2]
12.	$2p^5(^2P°_{1/2})3s'$–$2p^5(^2P°_{1\ 1/2})3p$	[1/2]°–[1 1/2] (5)	6532.9	11650	1.0×10^{17}	0.31	0.66	0.21	1.05	C	[4]
13.	$2p^53s'$–$2p^5(^2P°_{1/2})3p'$	[1/2]°–[1 1/2] (5)	6266.5	11650–13600	$(0.5–1.25) \times 10^{17}$	0.13–0.31	0.60–0.55			B	[2]
14.		[1/2]°–[1 1/2]	6163.6	11650–13600	$(0.5–1.25) \times 10^{17}$	0.12–0.30	0.55–0.53			B	[2]
15.	$2p^5(^2P°_{1/2})3s'$–$2p^5(^2P°_{1\ 1/2})3p$	[1/2]°–[1 1/2] (6)	6929.5	11650	1.0×10^{17}	0.40	0.76	0.27	1.93	C	[4]
16.	$2p^53s'$–$2p^5(^2P°_{1/2})3p'$	[1/2]°–[1 1/2] (6)	6717.0	11650	1.0×10^{17}	0.47	1.00	0.25	1.79	C	[4]

No.	Transition array	Transition (jl-coupling) (Multiplet)	Wavelength (Å)	Temperature (K)	Electron density (cm⁻³)	w_m(Å)	w_m/w_{th}	d_m(Å)	d_m/d_{th}	Acc.	Ref.
17.		[1/2]°–[1 1/2]	6678.3	11650	1.0×10^{17}	0.52	1.10	0.25	1.79	C	[4]
18.		[1/2]°–[1/2]	6599.0	11650	1.0×10^{17}	0.43	0.91	0.20	1.43	C	[4]
19.		[1/2]°–[1/2]	5852.5	11650–13600	$(0.5–1.25) \times 10^{17}$	0.38–0.70	1.61–1.10			B	[2]
20.	$2p^53p–2p^5(^2P°_{1\ 1/2})4d$	[1/2]–[1/2]° (9)	5441.1	11000	1.0×10^{17}	50.4		15.0		C	[3]
21.	$2p^53p–2p^5(^2P°_{1\ 1/2})4d$	[2 1/2]–[3 1/2]° (13)	5764.4	11000	1.0×10^{17}	31.0		12.4		C	[3]
22.	$2p^53p–2p^5(^2P°_{1\ 1/2})4d$	[2 1/2]–[3 1/2]° [19]	5820.2	11000	1.0×10^{17}	23.8		13.8		C	[3]

STARK WIDTHS AND SHIFTS

J. Phys. Chem. Ref. Data, Vol. 5, No. 2, 1976

243

7.14. Nitrogen

N I

Ground State $1s^2 2s^2 2p^3\ ^4S^\circ_{3/2}$

Ionization Potential   14.53 eV = 117214 cm^{-1}

Wavelength (Å)	No.	Wavelength (Å)	No.	Wavelength (Å)	No.	Wavelength (Å)	No.
1134.6	1	4214.7	18	7423.6	14	8655.9	15
1176.9	9	4215.9	18	7442.3	14	8680.3	12
1199.9	2	4223.0	18	7468.3	14	8603.4	12
1243.3	5	4224.7	18	8184.8	13	8686.2	12
1310.7	8	4230.4	18	8188.0	13	8703.3	12
1319.5	7	4384.4	24	8200.4	13	8711.7	12
1411.9	6	4391.3	24	8210.7	13	8718.8	12
1493.3	3	4914.9	20	8216.3	13	9028.9	22
1743.6	4	4935.0	20	8223.1	13	9045.9	17
4099.9	16	5281.2	11	8242.4	13	9049.5	17
4110.0	16	5328.7	10	8567.7	15	9049.9	17
4137.6	19	5401.4	21	8590.0	15	9060.7	22
4151.5	19	5411.9	21	8629.2	15	10130	23

An extensive number of experimental Stark broadening parameters exists for neutral nitrogen lines [1–6]. A number of measurements were performed in an atmospheric pressure pulsed arc [2, 3], but only at a single electron density and temperature. In refs. [1, 4–6] wall-stabilized arcs were used as the plasma source, and the line parameters were measured for a number of electron densities and temperatures. While the temperature range did not exceed 2,000 K in refs. [1, 4, 6], in ref. [5] it covers more than 12,000 K. Because of the large temperature range of experimental data, these results (multiplet 9, ref. [5]) are given in graphical form in figure 4, and the averaged extremes are listed in the data table.

In general there is good agreement between theory and experiment (within ±30 percent). The exceptions are vacuum uv lines and multiplet 18. Due to the experimental difficulties in measuring broadening parameters of uv lines and their usually small halfwidths, high accuracy is not expected for these measurements. However, for the broad 10130 Å line of multiplet 18, the experimental precision should be quite high. Unfortunately, it has not been clearly stated in ref. [2] how the measurements were performed. For example, a line with exactly this wavelength does not exist, the nearest one is 10128.3 Å line. Also, at the high electron concentration (1.6 × 10^{17} cm^{-3}) of this experiment, partial

blending with other lines of this multiplet is quite likely, and this may have produced the large measured halfwidth. However, only a new experiment can clear up this discrepancy.

The results which were reported in ref. [1] differ more than ±30 percent from the theory and from other experimental results. Since a direct independent method for the measurement of electron density was not employed in this experiment, a lower accuracy is assumed for these data.

The results of refs. [5] and [6] are averaged over each multiplet and are the same value for each line within a multiplet. The wavelengths of Nos. 1, 9, 2, 5, 8, 7, 3, and 4 are averaged values for the multiplet.

References

[1] Stampa, A., Z. Astrophys. 58, 82 (1963).
[2] Morris, J. C., Krey, R. U., and Garrison, R. L., AVCO Corporation, Space Systems Division, Report AVSSD-0049-68-RR (1968).
[3] Morris, J. C., and Garrison, R. L., Phys. Rev. 188, 112 (1969).
[4] Nubbemeyer, H., and Wende, B., Z. Angew. Phys. 27, 214 (1969).
[5] Shumaker, J. B., J. Quant. Spectrosc. Radiat. Transfer 14, 19 (1974), and private communication.
[6] Helbig, V., Kelleher, D. E., and Wiese, W. L., to be published (1974).

Key data on experiments

Ref.	Plasma source	Method of measurement		Remarks
		Electron density	Temperature	
[1]	Wall-stabilized arc	Plasma composition data	Absolute intensity of N I and N II lines	
[2]	Constricted generator Gerdin type	H_β	Intensity ratio of 4935 Å N I line to N continuum	
[3]	Constricted generator Gerdin type	H_β	Absolute intensities of Ar I and Ar II lines	
[4]	Wall-stabilized arc	H_β	Absolute intensities of Ar I and Ar II lines	
[5]	Wall-stabilized arc	Plasma composition data	Saha and Boltzmann equations	
[6]	Wall-stabilized arc	H_β	Absolute intensities of N I, Ar I, and Ar II lines	

Numerical results for N I

No.	Transition array	Transition (Multiplet)	Wavelength (Å)	Temperature (K)	Electron density (cm⁻³)	w_m(Å)	w_m/w_{th}	d_m(Å)	d_m/d_{th}	Acc.	Ref.
1.	$2s^22p^3-2s2p^4$	$^4S°-^4P$ (2 uv)	1134.6	13600	1.32×10^{17}	1.27×10^{-2}				C	[3]
2.	$2p^3-2p^2(^3P)3s$	$^4S°-^4P$ (1 uv)	1199.9	13600	1.32×10^{17}	1.32×10^{-2}	0.63			C	[3]
3.	$2p^3-2p^2(^3P)3s$	$^2D°-^2P$ (4 uv)	1493.3	13600	1.32×10^{17}	5.28×10^{-2}	1.49			C	[3]
4.	$2p^3-2p^2(^3P)3s$	$^2P°-^2P$ (9 uv)	1743.6ᵃ	13600	1.32×10^{17}	2.64×10^{-2}				C	[3]
5.	$2p^3-2p^2(^1D)3s'$	$^2D°-^2D$ (5 uv)	1243.3	13600	1.32×10^{17}	1.32×10^{-2}	0.56			C	[3]
6.	$2p^3-2p^2(^1D)3s'$	$^2P°-^2D$ (10 uv)	1411.9	13600	1.32×10^{17}	1.32×10^{-2}	0.44			C	[3]
7.	$2p^3-2p^2(^3P)3d$	$^2P°-^2P$ (12 uv)	1319.5	13600	1.32×10^{17}	1.08×10^{-2}	1.08			C	[3]
8.	$2p^3-2p^2(^3P)3d$	$^2P°-^2D$ (13 uv)	1310.7	13600	1.32×10^{17}	7.98×10^{-2}	0.64			C	[3]
9.	$2p^3-2p^2(^3P)4s$	$^2D°-^2P$	1176.9	13600	1.32×10^{17}	1.00×10^{-2}				C	[3]
10.	$2s2p^4-2s^22p^2(^3P)4p$	$^4P-^4D°$ (13)	5328.7	12500–14300 / 10300–12400	$(0.86-1.52) \times 10^{17}$ / $(2.0-8.2) \times 10^{16}$	2.0–3.6 / 0.5–2.0		0.34–0.58		C / B	[1] / [4]
11.	$2s2p^4-2s^22p^2(^3P)4p$	$^4P-^4P°$ (14)	5281.2	12500–14300	$(0.86-1.52) \times 10^{17}$	2.0–3.6		0.45–0.77		C	[1]
12.	$2p^23s-2p^2(^3P)3p$	$^4P-^4D°$ (1)	8718.8	13000	1.61×10^{17}	1.67	0.99			B	[2]
			8711.7	13000	1.61×10^{17}	1.67	0.99			B	[2]
			8703.3	13000	1.61×10^{17}	1.74	1.03			B	[2]
			8686.2	13000	1.61×10^{17}	1.74	1.03			B	[2]
			8683.4	13000	1.61×10^{17}	2.07	1.23			B	[2]
			8680.3	13000	1.61×10^{17}	1.93	1.18			B	[2]
13.	$2p^23s-2p^2(^3P)3p$	$^4P-^4P°$	8216.3	13000	1.61×10^{17}	1.55	0.86			B	[2]
				12040–14100	$(0.68-1.57) \times 10^{17}$	0.70–1.63	1.05–0.99			B	[6]
			8210.7	13000	1.61×10^{17}	1.73	0.96			B	[2]
				12040–14100	$(0.68-1.57) \times 10^{17}$	0.61–1.42	0.91–0.86			B	[6]
			8242.4	13000	1.61×10^{17}	1.77	0.98			B	[2]

No.	Transition array	Transition (Multiplet)	Wavelength (Å)	Temperature (K)	Electron density (cm⁻³)	w_m(Å)	w_m/w_{th}	d_m(Å)	d_m/d_{th}	Acc.	Ref.
			8223.1	13000	1.61×10^{17}	1.63	0.90			B	[2]
				12040–14100	$(0.68–1.57) \times 10^{17}$	0.60–1.39	0.90–0.84			B	[6]
			8184.8	13000	1.61×10^{17}	1.58	0.88			B	[2]
				12040–14100	$(0.68–1.57) \times 10^{17}$	0.66–1.52	0.99–0.92			B	[6]
			8188.0	13000	1.61×10^{17}	1.49	0.82			B	[2]
				12040–14100	$(0.68–1.57) \times 10^{17}$	0.63–1.45	0.94–0.88			B	[6]
			8200.4	12040–14100	$(0.68–1.57) \times 10^{17}$	0.59–1.36	0.88–0.82			B	[6]
14.	$2p^23s–2p^2(^3P)3p$	$^4P–^4S°$ (3)	7468.3	13000	1.61×10^{17}	1.52	0.86			B	[2]
				11270–14750	$(0.45–1.79) \times 10^{17}$	0.42–1.60	0.89–0.79	0.17–0.69	0.69–0.67	B	[6]
			7442.3	13000	1.61×10^{17}	1.49	0.84			B	[2]
				11270–14750	$(0.45–1.79) \times 10^{17}$	0.42–1.60	0.89–0.79	0.17–0.69	0.69–0.67	B	[6]
			7423.6	13000	1.61×10^{17}	1.49	0.84			B	[2]
				11270–14750	$(0.45–1.79) \times 10^{17}$	0.42–1.60	0.89–0.79	0.17–0.69	0.69–0.67	B	[6]
15.	$2p^23s–2p^2(^3P)3p$	$^2P–^2P°$ (8)	8629.2	13000	1.61×10^{17}	2.72	0.96			B	[2]
			8590.0	13000	1.61×10^{17}	2.56	0.91			B	[2]
			8655.9	13000	1.61×10^{17}	2.96	1.05			B	[2]
			8567.7	13000	1.61×10^{17}	2.61	0.92			B	[2]
16.	$2p(^3P)3s–2p(^1D)3p'$	$^2P–^2D°$ (10)	4110.0	10300–12400	$(2.5–8.1) \times 10^{16}$	2.0–7.2				B	[4]
				11700–13150	$(0.59–1.12) \times 10^{17}$	4.03–7.67		(−0.86)–(−1.58)		B	[6]
			4099.9	10300–12400	$(2.5–8.1) \times 10^{16}$	1.8–5.6				B	[4]
				11700–13150	$(0.59–1.12) \times 10^{17}$	4.03–7.67		(−0.86)–(−1.58)		B	[6]
17.	$2p^23s'–2p^2(^1D)3p'$	$^2D–^2F°$	9045.9	13000	1.61×10^{17}	5.40				B	[2]
			9049.5[a]	13000	1.61×10^{17}	5.40				B	[2]
			9049.9[a]	13000	1.61×10^{17}	5.40				B[3]	[2]
18.	$2p^23s–2p^2(^3P)4p$	$^4P–^4P°$ (5)	4230.4	10850–12400	$(2.5–8.1) \times 10^{16}$	0.62–1.43	1.16–1.05			B	[4]
			4224.7	10300–12150	$(2.0–7.3) \times 10^{16}$	0.30–1.05	0.98–0.86			B	[4]
			4223.0	10300–12450	$(2.0–8.3) \times 10^{16}$	0.35–1.26	1.20–0.90			B	[4]
			4215.9	10200–12400	$(1.9–8.2) \times 10^{16}$	0.32–1.25	1.10–0.91			B	[4]
			4214.7	10200–12400	$(1.9–8.2) \times 10^{16}$	0.35–1.30	1.20–0.97			B	[4]
19.	$2p^23s–2p^2(^3P)4p$	$^4P–^4S°$ (6)	4151.5	10500–12350	$(2.4–8.1) \times 10^{16}$	0.38–1.30	0.90–0.85			B	[4]
				11700–14160	$(0.59–1.49) \times 10^{17}$	0.90–2.32	0.83–0.78	0.39–0.98	0.97–0.93	B	[6]
			4137.6	10600–12450	$(2.5–8.3) \times 10^{16}$	0.42–1.40	0.95–0.89			B	[4]
				11700–14160	$(0.59–1.49) \times 10^{17}$	0.90–2.32	0.83–0.78	0.39–0.98	0.97–0.93	B	[6]
			4143.4	11700–14160	$(0.59–1.49) \times 10^{17}$	0.90–2.32	0.83–0.78	0.39–0.98	0.97–0.93	B	[6]

J. Phys. Chem. Ref. Data, Vol. 5, No. 2, 1976

248

N. KONJEVIC AND J. R. ROBERTS

Numerical results for N ɪ—Continued

No.	Transition array	Transition (Multiplet)	Wavelength	Temperature (K)	Electron density (cm⁻³)	w_m(Å)	$w_{m'}$/th	d_m(Å)	d_m/d_{th}	Acc.	Ref.
20.	$2p^23s-2p^2(^3P)4p$	$^2P-^2S°$ (9)	4935	10650-12200	$(2.7-8.0) \times 10^{16}$	0.60-1.70	1.01-0.90			B	[4]
				11700-14640	$(0.59-1.64) \times 10^{17}$	1.18-3.50	0.88-0.85	(-0.20)-(-0.46)	0.86-0.73	B	[6]
				12000-24000	$(0.83-1.59) \times 10^{17}$	1.6-3.5				C	[5]
			4913.?	12500-14300	$(0.86-1.52) \times 10^{17}$	1.9-3.4	0.94-0.90	(-0.25)-(-0.43)	0.74-0.74	C	[1]
				11050-14500	$(0.40-1.62) \times 10^{17}$	0.85-3.46	0.96-0.85	(-0.15)-(-0.60)	0.95-0.96	B	[6]
				12000-24000	$(0.83-1.59) \times 10^{17}$	1.6-3.5				C	[5]
21.	$2p^2(^3P)3p-2p^2(^1S)3s''$	$^2P°-^2S$	5401.?	12500-14300	$(0.86-1.52) \times 10^{17}$	0.56-1.00		(-0.23)-(-0.39)		C	[1]
				11700-14640	$(0.59-1.64) \times 10^{17}$	0.35-0.97		(-0.18)-(-0.52)		B	[6]
			5411.9	11700-14640	$(0.59-1.64) \times 10^{17}$	0.35-0.97		(-0.18)-(-0.52)		B	[6]
22.	$2p^23p-2p^2(^3P)3d$	$^2S°-^2P$	9060.7	13000	1.61×10^{17}	3.13	1.13			B	[2]
				11750-14250	$(0.61-1.52) \times 10^{17}$	2.23-5.11	0.85-0.73	1.13-2.86	0.84-0.84	B	[6]
			9028.9	13000	1.61×10^{17}	7.02	0.97			B	[2]
				11750-14250	$(0.61-1.52) \times 10^{17}$	2.23-5.11	0.85-0.73	1.13-2.86	0.84-0.84	B	[6]
23.	$2p^23p-2p^2(^3P)3d$	$^4D°-^4F$ (18)	10130.0	13000	1.61×10^{17}	14.30	1.70			D	[2]
24.	$2p^2(^3P)3p-2p^2(^1D)3d'$	$^2P°-^2S$	4391.3	12500-14300	$(0.86-1.52) \times 10^{17}$	0.80-1.40		0.20-0.32		C	[1]
				11700-14640	$(0.59-1.64) \times 10^{17}$	0.48-1.56		0.22-0.57		B	[6]
			4384.4	11700-14640	$(0.59-1.64) \times 10^{17}$	0.48-1.56		0.22-0.57		B	[6]

ᵃ Blended for experimental results given.

7.15. Oxygen

O I

Ground State	$1s^22s^22p^4\ {}^3P_2$
Ionization Potential	$13.614\ eV\ =\ 109836.7\ cm^{-1}$

Wavelength (Å)	No.	Wavelength (Å)	No.	Wavelength (Å)	No.	Wavelength (Å)	No.
1303.5	1	6046.4	14	7473.2	3	18243.6	17
3692.4	7	6157.3	9	7476.4	3	26520.4	18
3947.3	5	6455.0	10	7477.2	3	27645.5	15
4368.3	6	6653.8	4	7479.1	3	28930.0	8
5329.0	12	7156.8	2	7480.7	3	30973.0	19
5436.8	13	7254.4	11	18021.2	16		

Various plasma sources were used for the investigation of neutral oxygen lines [1–5]. With the exception of ref. [1], H_β was used in the determination of electron density. In ref. [2], measurements of the complete profiles of two strongly broadened oxygen lines (6455.0 Å and 6046.4 Å) are reported, and they are further discussed in ref. [6].

Generally good agreement was found between theory and experiment (within ±30 percent) in the measured electron temperature range. The only exceptions are the results of ref. [1], which are systematically much smaller compared to the theory and other experimental results. However, this disagreement is still within the limits of our estimated accuracies. The result given for multiplet 55 is a single value given for all lines within the multiplet as stated in ref. [1]. The wavelengths of Nos. 1, 9, and 10 are averaged values for the multiplet.

It should also be noted that a large discrepancy with the theory exists for the shift of the 3947.3 Å line. Measurements in this particular case were taken near the temperature, where theoretical shift changes from red to blue, and it had a very small absolute value (∼0.01 Å), which could produce this large ratio. Therefore, even small variations in the theoretical computations (compare the theoretical results of ref. [7] and

ref. [8]) may introduce large variations of d_m/d_{th} shift ratio values in this temperature range.

In ref. [3] the w_m reported is actually obtained from a measurement of the product of the Stark width, w_m, and the oscillator strength, f, of the 1303.5 Å O I line. Therefore, the resultant w_m and uncertainty depends on the value of f.

It may be noted that in general for the few w_m/w_{th} ratios that have a temperature spread, this ratio decreases with increasing temperature. It should be noted also that the A value (see section 3) is greater than 0.5 for 5329.0 Å transition; however, eq (15) is used to determine the theoretical width for comparison.

References

[1] Jung, M., Z. Astrophys. 58, 93 (1963).
[2] Wiese, W. L., and Murphy, P. W., Phys. Rev. 131, 2108 (1963).
[3] Morris, J. C., and Garrison, R. L., Phys. Rev. 188, 112 (1969).
[4] Miller, M. H., and Bengtson, R. D., Phys. Rev. A 1, 983 (1970).
[5] Assous, R., J. Quant. Spectrosc. Radiat. Transfer 10, 975 (1970).
[6] Wiese, W. L., in Plasma Diagnostic Techniques, Ed. R. H. Huddlestone and S. L. Leonard, Ch. 6, Academic Press Inc., New York. (1965).
[7] Griem, H. R., Plasma Spectroscopy, McGraw-Hill Book Co., New York, (1964).
[8] Griem, H. R., Spectral Line Broadening by Plasmas, Academic Press, New York, (1974).

Key data on experiments

Ref.	Plasma source	Method of measurement		Remarks
		Electron density	Temperature	
[1]	Wall-stabilized arc	Plasma composition data	Absolute intensity of O I λ = 6654 Å line	Absorption checked with dispersion profile Carbon arc calibration
[2]	Wall-stabilized arc	H_β	Absolute intensity of O I lines	

Key data on experiments—Continued

Ref.	Plasma source	Method of measurement		Remarks
		Electtron densiy	Temperature	
[3]	Constricted generator Gerdin type	H_β	Absolute intensity of Ar I and Ar II lines	
[4]	Gas-driven shock tube	H_β	Absolute line intensity of Ne I 5852.5 Å and H_β; line reversal applied to H_α	
[5]	RF discharge	H_β	Plasma composition data	

No.	Transition array	Transition (Multiplet)	Wavelength (Å)	Temperature (K)	Electron density (cm^{-3})	w_m(Å)	w_m/w_{th}	d_m(Å)	d_m/d_{th}	Acc.	Ref.
1.	$2p^4$–$2p^3(^4S°)3s$	^3P–$^3S°$ (2 uv)	1303.5	13600	1.32×10^{17}	18.48×10^{-3}	0.76			D	[3]
2.	$2p^33s'$–$2p^3(^2D°)3p$	$^1D°$–^1D (38)	7156.8	11800–13800	$(0.49$–$1.11) \times 10^{17}$	0.37–0.85				C	[1]
3.	$2p^33s''$–$2p^3(^2P°)3p''$	$3P°$–^3D (55)	7473.2 7476.4 7477.2 7479.1 7480.7	11800–13800	$(0.49$–$1.11) \times 10^{17}$	0.37–0.87		0.66–1.22		C	[1]
4.	$2p^33s''$–$2p^3(^2P°)3p''$	$^1P°$–^1S (65)	6653.8	11800–13800	$(0.49$–$1.11) \times 10^{17}$	0.32–0.53				C	[1]
5.	$2p^33s$–$2p^3(^4S°)4p$	$^5S°$–^5P (3)	3947.3	12080	5.7×10^{16}	0.83	1.05	−0.13	11.92	B	[2]
6.	$2p^33s$–$2p^3(^4S°)4p$	$^3S°$–^3P (5)	4368.3	12080 11800–13800	5.7×10^{16} $(0.49$–$1.11) \times 10^{17}$	1.08 0.59–1.36	1.02 0.66–0.62	0.20 0.16–0.36	0.87 0.81–0.79	B C	[2] [1]
7.	$2p^3(^4S°)3s$–$2p^35p$	$^3S°$–^3P (6)	3692.4	12080	5.7×10^{16}	2.72		0.18		C	[2]
8.	$2p^3(^2P)4s$–$2p^3(^2P)4p$	$^3P°$–^3P	28930.0	11200	2.91×10^{16}	21.0				C	[5]
9.	$2p^33p$–$2p^3(^4S°)4d$	^5P–$^5D°$ (10)	6157.3	11000 11800–13800	1.0×10^{17} $(0.45$–$1.11) \times 10^{17}$	37.2 5.05–12.2	1.23 0.35–0.36	4.3–9.9	0.75–0.74	D D	[4] [1]
10.	$2p^33p$–$2p^3(^4S°)5s$	^5P–$^5S°$ (9)	6455.0	9500–12080 11800–13800	$(1.0$–$5.7) \times 10^{16}$ $(0.49$–$1.11) \times 10^{17}$	1.5–5.7 6.5–14.5	1.39–0.88 0.53–0.49	1.05–4.20 5.6–12.4	1.20–1.19 0.97–0.92	B C	[2] [1]
11.	$2p^33p$–$2p^3(^4S°)5s$	^3P–$^3S°$ (20)	7254.4	12080 11200	5.7×10^{16} 2.91×10^{16}	8.9 3.6	0.98 0.79	5.3	1.21	B C	[2] [5]
12.	$2p^33p$–$2p^3(^4S°)5d$	^5P–$^5D°$ (12)	5329.0	11000	1.0×10^{17}	70.6	0.81			C	[4]
13.	$2p^33p$–$2p^3(^4S°)6s$	^5P–$^5S°$ (11)	5436.8	11000	1.0×10^{17}	27.2	1.10			C	[4]
14.	$2p^33p$–$2p^3(^4S°)6s$	^3P–$^3S°$ (22)	6046.4	9500–13500	$(1.0$–$6.0) \times 10^{16}$	4.0–21.4	1.37–1.08	1.8–9.5	1.28–1.05	B	[2]

No.	Transition array	Transition (Multiplet)	Wavelength (Å)	Temperature (K)	Electron density (cm⁻³)	w_m(Å)	w_m/w_{th}	d_m(Å)	d_m/d_{th}	Acc.	Ref.
15.	$2s^22p^3(^4S°)4s-2s^22p^34p$	$^5S°-^5P$	27645.5	11200	2.91×10^{16}	22.0				C	[5]
16.	$2s^23p^3(^4S°)3d-2s^22p^34f$	$^5D°-^5F$	18021.2	11200	2.91×10^{16}	37.4		-10.8		C	[5]
17.	$2s^22p^3(^4S°)3d-2s^22p^34f$	$^3D°-^3F$	18243.6	11200	2.91×10^{16}	42.7		-5.4		C	[5]
18.	$2s^22p^3(^4S°)4p-2s^22p^34d$	$^5P-^5D°$	26520.4	11200	2.91×10^{16}	107.5		42.9		C	[5]
19.	$2s^22p^3(^4S°)4p-2s^22p^34d$	$^3P-^3D°$	30973.0	11200	2.91×10^{16}	185.0				C	[5]

7.16. Phosphorus

P I

Ground State $1s^2 2s^2 2p^6 3s^2 3p^3 \; {}^4S^\circ_{3/2}$

Ionization Potential $11.0 \text{ eV} = 88560 \text{ cm}^{-1}$

In ref. [2] the 5515.9 Å line reported is actually the 5015.9 Å, $4s \; {}^4P_{3/2}-4p \; {}^4S^\circ_{3/2}$ transition, as presented in ref. [3]. The temperature and electron density of ref. [2] are normalized values.

The double value of accuracy (B, D) given in the table refers to the fact that the accuracy of the widths is B and that of the shift is D, as stated in ref. [1].

References

[1] Voigt, P. A., and Roberts, J. R., to be published.
[2] Miller, M. H., and Bengtson, R. D., Phys. Rev. A 1, 983 (1970).
[3] Martin, W. C., J. Opt. Soc. Am. 49, 1071 (1959).

Key data on experiments

Ref.	Plasma source	Method of measurement		Remarks
		Electron density	Temperature	
[1]	Wall-stabilized arc	H_β, H_α	Composition data and H_β	
[2]	Gas-driven shock tube	H_β	Absolute line intensity of Ne I 5852.5 Å and H_β	Photographic technique

Numerical results for P I

Transition array	Transition (Multiplet)	Wavelength (Å)	Temperature (K)	Electron density (cm^{-3})	w_m(Å)	w_m/w_{th}	d_m(Å)	d_m/d_{th}	Acc.	Ref.
$3p^3-3p^24s$	${}^2D^\circ-{}^2P$	2136.2	12700	9.3×10^{16}	0.084	1.18	0.059	1.42	B,D	[1]
	(4 uv)	2149.1	12700	9.3×10^{16}	0.082	1.16	0.039	0.95	B,D	[1]
	${}^2P^\circ-{}^2P$	2534.0	12700	9.3×10^{16}	0.111	1.11	0.056	0.95	B,D	[1]
	(8 uv)	2535.6	12700	9.3×10^{16}	0.110	1.10	0.066	1.13	B,D	[1]
		2553.3	12700	9.3×10^{16}	0.111	1.11	0.057	0.97	B,D	[1]
		2554.9	12700	9.3×10^{16}	0.110	1.10	0.060	1.03	B,D	[1]
$3p^24s-3p^24p$	${}^4P-{}^4S^\circ$	5015.9	11000	1.0×10^{17}	11.8	1.22	4.6	−1.64ª	C	[2]
$3p^24s-3p^25p$	${}^4P-{}^4S^c$	5079.4	8400	0.78×10^{16}	0.45	0.64	0.18	−0.215ª	B,D	[1]
	${}^2P-{}^2P^\circ$	5345.9	8400	0.78×10^{16}	0.47	0.71	0.22	0.62	B,D	[1]
	${}^2P-{}^2D^\circ$	5458.3	8400	0.78×10^{16}	0.50	0.70	0.039	−0.282ª	B,D	[1]

ª Shift in direction opposite to theory.

7.17. Silicon

Si I

Ground State $1s^2 2s^2 2p^6 3s^2 3p^2 \; {}^3P_0$

Ionization Potential $8.151 \text{ eV} = 65747.5 \text{ cm}^{-1}$

With the exception of two lines [1], most of the experimental data were obtained in shock tubes, either gas-driven [2] or electrical [3].

The experimental results for the line widths of the multiplets 1 uv, 43 uv, and 3 differ appreciably from the theoretical values, while the shifts agree within the

limits of experimental error. Although an attempt is made in ref. [3] to correct for self-absorption, there are strong indications that self-absorption may still be a partial cause of this discrepancy. First, the disagreement with the theory decreases as the energy level of the transition increases (the highest self-absorption effect is expected for the transitions with energy levels nearest to the ground state). Secondly, the experimental shifts agree with the theory, and these measurements are not in their nature affected by self-absorption. Since the results of refs. [1] and [3] have such large differences, new data are very desirable.

The results of refs. [1] and [2] are normalized to $N_e = 1.0 \times 10^{18}$ and $N_e = 1.0 \times 10^{17}$, respectively. The conditions of refs. [1] and [3] result in a value of $R > 0.8$ (see section 3); however, eqs (15) and (16) were used to determine the theoretical widths and shifts for comparison.

The double accuracy (D, C) given in the table for ref. [3] denotes the accuracy for the widths is D and that of the shifts is C.

References

[1] Meyer, J., and Beck, R. J., Astron. Astrophys. 8, 93 (1970).
[2] Miller, M. H., and Bengtson, R. D., Phys. Rev. A 1, 983 (1970)
[3] Puric, J., Djenize, S., Labat, J., and Cirkovic, Lj., Z. Phys. 267, 71 (1974); Phys. Lett. A 45, 97 (1973).

Key data on experiments

Ref.	Plasma source	Method of measurement		Remarks
		Electron density	Temperature	
[1]	Hydrogen plasma jet	H_β	Plasma composition data	
[2]	Gas-driven shock tube	H_β	Absolute line intensity of Ne I 5852.5 Å and H_β; line reversal technique applied to H_α	Photographic technique
[3]	Electric T-tube	Laser interferometry	Relative intensities of Ar II lines	

Numerical results for Si I

Transition array	Transition (Multiplet)	Wavelength (Å)	Temperature (K)	Electron density (cm⁻³)	w_m(Å)	w_m/w_{th}	d_m(Å)	d_m/d_{th}	Acc.	Ref.
$3p^2\text{-}3p(^2P°)4s$	$^3P\text{-}^3P°$ (1 uv)	2506.9	8700–16400	$(2.9\text{-}5.7) \times 10^{17}$	0.79–1.60	2.72–2.68	0.14–0.34	0.86–0.92	D,C	[3]
		2514.3	8700–16400	$(2.9\text{-}5.7) \times 10^{17}$	0.79–1.71	2.72–2.87	0.14–0.40	0.86–1.07	D,C	[3]
		2516.1	8700–16400	$(2.9\text{-}5.7) \times 10^{17}$	0.79–1.71	2.72–2.87	0.14–0.34	0.86–0.92	D,C	[3]
		2519.2	8700–16400	$(2.9\text{-}5.7) \times 10^{17}$	0.87–1.60	3.12–2.68	0.20–0.34	1.20–0.92	D,C	[3]
		2524.1	8700–16400	$(2.9\text{-}5.7) \times 10^{17}$	0.87–1.60	3.12–2.68	0.14–0.40	0.86–1.07	D,C	[3]
		2528.5	8700–16400	$(2.9\text{-}5.7) \times 10^{17}$	0.87–1.71	3.12–2.87	0.14–0.34	0.86–0.92	D,C	[3]
$3p^2\text{-}3p(^2P°)4s$	$^1D\text{-}^1P°$ (43 uv)	2881.6	8709–16400	$(2.9\text{-}5.7) \times 10^{17}$	0.75–1.94	1.99–2.20	0.17–0.40	0.75–0.77	D,C	[3]
			12000	1.0×10^{18}	6.22	4.34	0.93	1.08	D	[1]
$3p^2\text{-}3p(^2P°)4s$	$^1S\text{-}^1P°$ (3)	3905.5	8700–16400	$(2.9\text{-}5.7) \times 10^{17}$	1.10–1.82	1.58–1.19	0.35–0.63	0.75–0.78	D,C	[3]
			12000	1.0×10^{18}	1.76	0.68	1.26	0.96	D	[1]
$3p4s\text{-}3p(^2P°)5p$	$^3P°\text{-}^3P$ (10)	5645.6	11000	1.0×10^{17}	7.4	1.14			C	[2]
		5665.6	11000	1.0×10^{17}	7.3	1.12			C	[2]
		5690.4	11000	1.0×10^{17}	7.7	1.18			C	[2]
		5701.1	11000	1.0×10^{17}	6.5	1.01			C	[2]
		5708.4	11000	1.0×10^{17}	7.1	1.09			C	[2]
$3p4s\text{-}3p(^2P°)5p$	$^3P°\text{-}^3S$ (11)	5684.5	11000	1.0×10^{17}	1.54	1.54			C	[2]
$3p4s\text{-}3p(^2P°)5p$	$^1P°\text{-}^1D$ (16)	5948.6	11000	1.0×10^{17}	1.01	1.01			C	[2]

7.18. Sodium

Na I

Ground State $1s^2 2s^2 2p^6 3s\ ^2S_{1/2}$

Ionization Potential   5.138 eV = 41449.65 cm^{-1}

Of the eight papers reviewed, only ref. [1] contains sufficient information to be considered for analysis. Four transitions from two multiplets were analyzed. Because both experimental and theoretical results are not given for separate lines within a multiplet, single values of w_m are listed for each multiplet. Although a sufficiently large temperature range is covered in the experiment to indicate some dependence of w_m/w_{th} on temperature, w_m has so much experimental scatter that it prevented a meaningful analysis. Therefore, an average value is given for w_m/w_{th} for the data of [1]. It should

be noted that while a temperature range is listed, the extremes of this range do not correspond to the extremes in the electron density range. However, the extreme values of the range listed for w_m do correspond to the extreme values of the electron density range. For the actual temperature—electron density correspondence—the reader is referred to [1].

References

[1] Oettinger, P. E. and Cooper, J., J. Quant. Spectrosc. Radiat. Transfer 9, 591 (1969).

Key data on experiments

Ref.	Plasma source	Method of measurement		Remarks
		Electron density	Temperature	
[1]	Combination of oven and linear pinch discharge	He I 3888.7 Å halfwidth	Relative intensities of He I lines	

Numerical results for Na I

Transition array	Transition (Multiplet)	Wave-length (Å)	Temperature (K)	Electron density (cm^{-3})	w_m(Å)	w_m/w_{th}	d_m(Å)	d_m/d_{th}	Acc.	Ref.
3p–4d	$^2P°–^2D$ (6)	5682.6 5688.2	11120–19750[a]	(0.94–1.70) × 10^{16}	3.7–6.9	1.03[b]			D	[1]
3p–5d	$^2P°–^2D$ (9)	4978.5 4982.8	11120–19750[a]	(0.94–1.70) × 10^{16}	4.1–5.8	0.34[b]			D	[1]

[a] Extremes of temperature range do not correspond to extremes of N_e range.
[b] Average value for range of T and N_e.

7.19. Sulfur

S I

Ground State $1s^2 2s^2 2p^6 3s^2 3p^4\ ^3P_2$

Ionization Potential   10.357 eV = 83559.3 cm^{-1}

Stark broadening data of sulfur lines have been obtained with two different plasma sources, a wall-stabilized arc [1] and a gas-driven shock tube [2]. Both sets of results agree with the theory well within the uncertainty limits. The only exception is the shift of lines belonging to multiplet no. 8, where the results of ref. [2] differ by more than 50 percent from the theory and the other experiment [1].

The results of ref. [2] are normalized to $N_e = 1.0 \times 10^{17}$ cm^{-3} and $T = 11000$ K.

References

[1] Bridges, J. M., and Wiese, W. L., Phys. Rev. 159, 31 (1967).
[2] Miller, M. H., and Bengtson, R. D., Phys. Rev. A 1, 983 (1970).

Key data on experiments

Ref.	Plasma source	Method of measurement		Remarks
		Electron density	Temperature	
[1]	Wall-stabilized arc	H_β	Absolute intensities of O I lines	
[2]	Gas-driven shock tube	H_β	Absolute line intensity of Ne I 5852.5 Å and H_β; line reversal technique applied to H_α	Photographic technique

Numerical results for S I

Transition array	Transition (Multiplet)	Wavelength (Å)	Temperature (K)	Electron density (cm^{-3})	w_m(Å)	w_m/w_{th}	d_m(Å)	d_m/d_{th}	Acc.	Ref.
$3p^34s-3p^3(^4S°)4p$	$^5S°-^5P$ (1)	9223.4^a	12200	6.3×10^{16}	1.5	1.05			B	[1]
$3p^34s-3p^3(^4S°)4p$	$^3S°-^3P$ (3)	10456.0^a	12200	6.3×10^{16}	2.3	1.23			B	[1]
$3p^34s-3p^3(^4S°)5p$	$^5S°-^5P$ (2)	4695.1^a	11200	7.0×10^{16}	3.4	1.06	1.7	1.12	B	[1]
			11000	1.0×10^{17}	5.3	1.15	2.7	1.24	C	[2]
$3p^34s-3p^3(^4S°)5p$	$^3S°-^3P$ (4)	5278.7^a	11200	7.0×10^{16}	3.0	0.98			B	[1]
			11000	1.0×10^{17}	4.8	1.10	2.3	1.12	C	[2]
$3p^34p-3p^3(^4S°)5d$	$^5P-^5D°$ (8)	6751.2^a	11400	7.5×10^{16}	26.0	1.12	1.0	0.88	B	[1]
			11000	1.0×10^{17}	31.8	1.04	2.3	1.55	C	[2]

^{a} Average wavelength of a blended multiplet.

7.20. Xenon

Xe I

Ground State $1s^22s^22p^63s^23p^63d^{10}4s^24p^64d^{10}5s^25p^6$ $^1S_0$

Ionization Potential 12.127 eV = 97834.4 cm^{-1}

A gas-driven shock tube was used as a source in an experiment to determine Stark widths of xenon lines [1]. However, there are no theoretical data for comparison. The temperature remained essentially constant over the range of electron density as stated in ref. [1].

Reference

[1] Lesage, A. and Richou, J., J. Quant. Spectrosc. Radiat. Transfer 12, 1313 (1972).

Key data on experiments

Ref.	Plasma source	Method of measurement		Remarks
		Electron density	Temperature	
[1]	Gas-driven shock tube	Laser interferometry	Plasma composition data	Photographic technique

Numerical results for Xe I

Transition array	Transition (jl-coupling) (Multiplet)	Wave-length (Å)	Temper-ature (K)	Electron density (cm^{-3})	w_m(Å)	w_m/w_{th}	d_m(Å)	d_m/d_{th}	Acc.	Ref.
$5p^5(^2P°_{1\,1/2})6s-$	[1 1/2]°–[1/2]	4582.7	10000	$(2.1-5.4) \times 10^{16}$	1.78–4.72				C	[1]
$5p^5(^2P°_{1/2})6p'$	[1 1/2]°–[1 1/2]	4734.2	10000	$(2.6-7.0) \times 10^{16}$	0.40–0.74				C	[1]
$5p^5 6s-$	[1 1/2]°–[1 1/2]	4624.3	10000	$(2.1-7.0) \times 10^{16}$	1.39–4.70				C	[1]
$5p^5(^2P°_{1\,1/2})7p$	[1 1/2]°–[2 1/2]	4671.2	10000	$(2.1-7.0) \times 10^{16}$	1.20–4.04				C	[1]
	[1 1/2]°–[2 1/2]	4697.0	10000	$(2.6-7.0) \times 10^{16}$	1.43–3.97				C	[1]

7.21. Zinc

Zn I

Ground State $1s^2 2s^2 2p^6 3s^2 3p^6 3d^{10} 4s^2\ {}^1S_0$

Ionization Potential 9.391 eV = 75766.8 cm^{-1}

Only one paper reports measurements of Stark broadening parameters of neutral zinc lines [1], and there are no theoretical data for comparison. All results are normalized in ref. [1] to $N_e = 1.0 \times 10^{17}$ cm^{-3} and $T = 11,000$ K. Comparisons within various multiplets reveal for the same experimental conditions large variations in the widths. This may be caused by improper treatment of self-absorption, especially for the stronger lines. The weaker lines which are least affected by this effect,

exhibit the smallest widths. In multiplet no. 5 uv, there are blended lines within the multiplet separated by 0.1–0.2 Å, but because the actual experimental electron densities were in the range $(1.0-7.0) \times 10^{17}$ cm^{-3}, these line widths were not too affected by this blending.

Reference

[1] Kusch, H. J., and Oberschelp, E., Z. Astrophys. 67, 77 (1967).

Key data on experiments

Ref.	Plasma source	Method of measurement		Remarks
		Electron density	Temperature	
[1]	Pulsed discharge	H$_\beta$	Plasma composition data	Photographic technique

Numerical results for Zn I

Transition array	Transition (Multiplet)	Wavelength (Å)	Temperature (K)	Electron density (cm^{-3})	w_m(Å)	w_m/w_{th}	d_m(Å)	d_m/d_{th}	Acc.	Ref.
$3d^{10}4s4p-3d^{10}4s(^2S)5s$	$^3P°-^3S$	4810.5	11000	1.0×10^{17}	1.65				D	[1]
	(2)	4722.2	11000	1.0×10^{17}	1.57				D	[1]
		4680.1	11000	1.0×10^{17}	0.84				D	[1]
$3d^{10}4s4p-3d^{10}4s(^2S)4d$	$^3P°-^3D$	3345.0	11000	1.0×10^{17}	1.74				D	[1]
	(4)	3302.6	11000	1.0×10^{17}	1.40				D	[1]
		3282.3	11000	1.0×10^{17}	0.91				D	[1]
$3d^{10}4s4p-3d^{10}4s(S)6s$	$^3P°-^3S$	3072.2	11000	1.0×10^{17}	0.70				D	[1]
	(5)	3035.8	11000	1.0×10^{17}	0.61				D	[1]
		3018.4	11000	1.0×10^{17}	0.56				D	[1]
$3d^{10}4s4p-4d^{10}4s(^2S)5d$	$^3P°-^3D$	2800.9[a]	11000	1.0×10^{17}	1.96				D	[1]
	(5 uv)	2770.9[a]	11000	1.0×10^{17}	2.49				D	[1]
		2756.5	11000	1.0×10^{17}	1.27				D	[1]

[a] Blended within multiplet.